Proteomics fingerprinting of phagosome maturation and evidence for the role of a Galpha during uptake

Gotthardt, Daniel; Blancheteau, Vincent; Bosserhoff, Armin; Ruppert, Thomas; Delorenzi, Mauro; Soldati, Thierry

How to cite

GOTTHARDT, Daniel et al. Proteomics fingerprinting of phagosome maturation and evidence for the role of a Galpha during uptake. In: Molecular & cellular proteomics, 2006, vol. 5, n° 12, p. 2228–2243. doi: 10.1074/mcp.M600113-MCP200

This publication URL: https://archive-ouverte.unige.ch/unige:18913
Publication DOI: 10.1074/mcp.M600113-MCP200

Proteomics Fingerprinting of Phagosome Maturation and Evidence for the Role of a Gα during Uptake*

Daniel Gotthardt,[a,b,c] Vincent Blancheteau,[c,d] Armin Bosserhoff,[e] Thomas Ruppert,[e] Mauro Delorenzi,[f,g,h] and Thierry Soldati[a,d,i,j]

Phagocytosis, whether of food particles in protozoa or bacteria and cell remnants in the metazoan immune system, is a conserved process. The particles are taken up into phagosomes, which then undergo complex remodeling of their components, called maturation. By using two-dimensional gel electrophoresis and mass spectrometry combined with genomic data, we identified 179 phagosomal proteins in the amoeba *Dictyostelium*, including components of signal transduction, membrane traffic, and the cytoskeleton. By carrying out this proteomics analysis over the course of maturation, we obtained time profiles for 1,388 spots and thus generated a dynamic record of phagosomal protein composition. Clustering of the time profiles revealed five clusters and 24 functional groups that were mapped onto a flow chart of maturation. Two heterotrimeric G protein subunits, Gα$_4$ and Gβ, appeared at the earliest times. We showed that mutations in the genes encoding these two proteins produce a phagocytic uptake defect in *Dictyostelium*. This analysis of phagosome protein dynamics provides a reference point for future genetic and functional investigations. ***Molecular & Cellular Proteomics 5:2228–2243, 2006.***

Phagocytosis is the complex process by which eukaryotes ingest large particles of over 200-nm diameter. Many primitive eukaryotic cells phagocytose food particles, whereas in metazoa so-called "professional phagocytes" like the neutrophils and macrophages of the immune system specialize in engulfing invading microorganisms and parasites as well as necrotic and apoptotic cell remnants. Usually phagocytosis is triggered by contact of the particle with the cell surface, which induces its actin-mediated engulfment into a membrane-bound phagosome derived from the plasma membrane. Other endomembrane compartments such as endosomes and the endoplasmic reticulum (ER)[1] contribute to the newly formed phagosomes. After killing of the engulfed microorganism, the contents of the phagosome are digested, and finally the lysosomal hydrolases are recycled for further use. During this maturation process, the phagosome remodels the protein and lipid components of its membrane as well as the soluble luminal components (1). Maturation of the phagosome is thus a normal part of its function, but the organelle can also be remodeled by some bacterial pathogens and eukaryotic parasites that "hijack" phagosomes and use them as a refuge where they can proliferate and evade the surveillance of the immune system (2).

Numerous studies have contributed to our understanding of the importance of many factors in phagosome maturation including phosphoinositides (3) and other lipids (4), small GTPases (5), signaling and actin dynamics (6, 7), and fusion with endocytic compartments (8, 9). Yet despite a century of study, the mechanisms of phagocytic uptake and maturation are still relatively poorly understood. Exciting progress has been made, however, since the advent of large scale proteomics methods, which have revealed new facets of this organelle (10). By combining two-dimensional (2D) gel electrophoresis with mass spectrometry, the first proteomics analysis of phagosomes from mouse macrophages identified over 140 proteins (11). This analysis found diverse protein classes including not only the expected lysosomal proteins but also a large variety of proteins involved in regulating membrane trafficking, such as SNAREs and Rab GTPases as well as a subset of heterotrimeric G protein subunits involved in signal transduction and many others (11). Despite these pioneering studies and recent technical advances, time-dependent organelle proteomics is still in its infancy. This is largely due to the paucity of appropriate bioinformatics tools to extract and integrate large scale and time-profiled proteomics data.

From the [a]Department of Molecular Cell Research, Max Planck Institute for Medical Research, [b]Department of Internal Medicine IV, University Hospital of Heidelberg, and [e]Zentrum für Molekulare Biologie der Universität Heidelberg (ZMBH), D-69120 Heidelberg, Germany, [d]Department of Biological Sciences, Imperial College, London SW7 2AZ, United Kingdom, [f]ISREC National Centre of Competence in Research (NCCR) Molecular Oncology, Swiss Institute of Experimental Cancer Research (ISREC), Epalinges, CH-1006 Switzerland , [g]ISREC Swiss Institute of Bioinformatics (SIB), CH-1015 Lausanne, Switzerland, and [i]Département de Biochimie, Faculté des Sciences, Université de Genève, CH-1211 Genève-4, Switzerland

Received April 3, 2006, and in revised form, August 10, 2006

Published, MCP Papers in Press, August 22, 2006, DOI 10.1074/mcp.M600113-MCP200

[1] The abbreviations used are: ER, endoplasmic reticulum; 2D, two-dimensional; NSF, *N*-ethylmaleimide-sensitive factor; SNARE, soluble NSF attachment protein receptor; PMF, peptide mass fingerprint; HSP, heat shock protein.

Supplemental Material can be found at: http://www.mcponline.org/cgi/content/full/M600113-MCP200/DC1

The social amoeba *Dictyostelium* is a very effective phagocyte, and its experimental versatility makes it an ideal candidate for multidisciplinary studies of cell function. Its genome is fully sequenced, assembled, and thoroughly and accurately annotated (12), confirming that amoebae are the closest group to metazoa and fungi. Large scale analyses are now possible in *Dictyostelium* by random insertion of plasmid sequences (13), microarrays (14), and proteomics (15, 16). *Dictyostelium* is also a well established model organism in which to study interactions between the host cell and a variety of human pathogens (17) including *Legionella* (18, 19), *Mycobacterium* (20), and *Pseudomonas aeruginosa* (21, 22). Furthermore the morphology and mechanisms of macropinocytosis and phagocytosis in *Dictyostelium* are very similar to those in metazoa (16, 23–26). Protozoan amoebae in general are natural hosts for bacterial pathogens and can be made to host experimental species of bacteria (27). Proteomics studies of phagosomes isolated from the amoeba *Entamoeba histolytica*, for example, have revealed several aspects of phagosome signaling, uptake mechanisms, and time-dependent maturation in common with phagocytosis in mammalian professional phagocytes (28–31). Interestingly as in mouse phagosomes, a subset of heterotrimeric G protein subunits were identified in the phagosomes of *E. histolytica* (31).

Here we used a combination of time-resolved 2D gel electrophoresis and mass spectrometry-assisted protein identification to generate a protein history of the life of a phagosome in *Dictyostelium*, incorporating 179 phagosomal components. By clustering proteins that appear and disappear from the phagosome at similar times, we defined groups of proteins and functions that can be placed on a flow chart of phagosome maturation. Validating this approach, we found that two heterotrimeric G protein subunits, Gα_4 and Gβ belong to two distinct but related groups of proteins present at early times in phagosome maturation. By studying *Dictyostelium* strains with ablations of the genes encoding Gα_4 and Gβ using a flow cytometry-based assay for phagocytic uptake, we demonstrated that both Gα_4 and Gβ function in an early step of phagocytosis.

EXPERIMENTAL PROCEDURES

Cell Culture—*Dictyostelium discoideum* cells of wild-type strain Ax2 were grown axenically in HL5c medium (32) supplemented with 10 units/ml penicillin and 10 μg/ml streptomycin on plastic dishes or in shaking culture (at 180 rpm) at 22 °C. Mutant cell lines were selected and grown in HL5c medium supplemented with 5 μg/ml G418.

Antibodies—The antibodies used in this study were mouse monoclonal antibodies and rabbit polyclonal antibodies raised against *Dictyostelium* proteins as listed in Supplemental Table SII.

Quantitative Immunoblotting—After SDS-PAGE (33) and transfer onto nitrocellulose membranes (Protran, Schleicher & Schuell), immunodetection was performed as described previously using horseradish peroxidase-coupled goat anti-mouse or goat anti-rabbit IgGs (BioRad) at 1:5,000 dilution (34). Detection was performed with ECL Plus (Amersham Biosciences) using a chemiluminescence imager (LAS-1000, Fuji Film). Data quantification was carried out with Image Gauge version 3.0 (Fuji Film).

Buffers—Soerensen buffer contained 15 mM KH_2PO_4, 2 mM Na_2HPO_4, pH 6. Homogenization buffer contained 20 mM HEPES-KOH, pH 7.2, 0.25 M sucrose, 1× Complete™ EDTA-free protease inhibitor (Roche Applied Science). Membrane buffer contained 20 mM HEPES-KOH, pH 7.2, 20 mM KCl, 2.5 mM $MgCl_2$, 1 mM DTT, 20 mM NaCl. Storage buffer contained 25 mM HEPES-KOH, pH 7.2, 1.5 mM magnesium acetate, 1 mM $NaHCO_3$, 1 μM $CaCl_2$, 25 mM KCl, 1 mM ATP, 1 mM DTT, 1× Complete EDTA-free protease inhibitor, 100 mM sucrose.

Isolation of Phagosomes—Phagosomes were prepared as described before (16, 35) and as briefly outlined in the supplemental information.

Carbonate Extraction—Carbonate extraction of phagosome membranes was carried out as described previously (36). In brief, freshly prepared phagosome pellets (about 7×10^{10} phagosomes prepared from 1.5×10^9 cells containing an average of 46.7 beads/cell) were resuspended in carbonate buffer (200 mM Na_2CO_3 (Sigma), pH 11) by vortexing. After homogenization by five passages through the needle of a 1-ml insulin syringe, samples were kept on ice for 1 h. Stripped phagosome membranes were repelleted by ultracentrifugation for 1 h at 100,000 × *g* in a Beckmann MLA130 rotor. Pellets were resuspended in lysis buffer containing 7 M urea (GE Healthcare), 2 M thiourea (Amersham Biosciences), 2% (w/v) CHAPS (Calbiochem), 2% (w/v) ASB-C8Ø (Calbiochem), 1% (w/v) DTT (Pharmacia Biotech), 2% (v/v) ampholytes (IPG buffer, pH 3–10 non-linear, Amersham Biosciences), and a protease inhibitor mixture (Complete EDTA-free). After sonication, isoelectric focusing gel electrophoresis was carried out as described below. Supplemental information is available.

Sample Preparation and 2D Gel Electrophoresis—Intact purified phagosomes were resuspended in lysis buffer containing 7 M urea (Merck), 2 M thiourea (Merck), 2% (w/v) CHAPS (Sigma), 1% (w/v) DTT (Sigma), 2% (v/v) Pharmalyte pH 3–10 (Amersham Biosciences), and a protease inhibitor mixture (Complete EDTA-free, Roche Applied Science) (37, 38). Suspensions were sonicated 3 × 10 min at 4 °C in a bath sonicator, incubated at room temperature for 2 h, and centrifuged for 60 min at 75,000 × *g* in a Beckmann TL120 centrifuge, and supernatants were stored at −80 °C until further use.

Extracts were separated in the first dimension using 18-cm strips with immobilized non-linear gradients from pH 3–10 pH (Amersham Biosciences) followed by standard SDS-PAGE as described previously (37, 39–42) with minor modifications described in the supplemental information. 2D gels were either stained with silver (43) or with colloidal Coomassie Blue (Novex/Invitrogen) according to the manufacturer's instructions. The gels were scanned using a Sharp JX-330 scanner and Imagemaster Labscan software. Procedures were carried out under standardized conditions for all gels. Supplemental information is available.

Mass Spectrometry—Individual spots were excised from 2D gels, reduced with DTT, alkylated with iodoacetamide, and digested with trypsin as described previously (44). Following digestion, tryptic peptides were extracted from the gel pieces with 50% acetonitrile, 0.1% TFA; concentrated; and analyzed by mass spectrometry.

For peptide fingerprinting by MALDI-TOF mass spectrometry (Ultraflex, Bruker), samples were desalted using ZipTip (Millipore) according to the manufacturer's instructions and spotted onto a steel target using α-cyano-4-hydroxycinnamic acid as matrix. The peptide mass fingerprint (PMF) was acquired after external calibration (peptide calibration standard II, Bruker) in positive ion reflector mode. For protein identification by PMF, peptide masses were labeled manually using the SNAP algorithm (signal to noise ratio = 3; quality factor threshold, 100) (flexAnalysis, Bruker) by comparison with a control sample taken from a spot of an empty area of the same gel. The PMF

was searched against the *Dictyostelium* database (protein sequences for dictyBase primary features, 13,676 sequences, at dictybase.org) using Mascot version 2.0.5 (Matrix Science). The algorithm was set to use trypsin as the enzyme, allowing for one missed cleavage site and assuming carbamidomethyl as a fixed modification of cysteine and oxidized methionine as a variable modification. Mass tolerance was set to 100 ppm unless otherwise indicated. Protein hits were considered identified if the Mascot score exceeded the significance level ($p > 0.05$).

For peptide sequencing by ESI Q-TOF mass spectrometry, peptides were desalted and concentrated using custom-made chromatographic columns (Poros 50 R2, Perseptive Biosystems) (45). They were eluted directly into a precoated borosilicate nanoelectrospray needle (MDS Protana, Odense, Denmark). Mass spectrometry was performed on a Q-TOF mass spectrometer (PE Sciex, Weiterstadt, Germany) equipped with a nano-ESI ion source (MDS Protana). A potential of 900 V was applied to the nanoelectrospray needle. Declustering potential and focusing potential were set to 40 and 100, respectively. Fragmentation of selected peptides (unit resolution) was usually performed at three different collision energies (22, 27, and 35 V). The data were processed using the Bioanalyst software (PE Sciex).

Image Processing and Dataset and Statistical Analyses—The digitalized 2D gels of the time series were analyzed using the Phoretix 2D Evolution (version 2005) software (Nonlinear Dynamics, Newcastle-upon-Tyne, UK) for spot detection, gel matching, and background correction (mode of nonspot, vector size 100 pixel), and these data were normalized to the sum of the total spot volume. Data were exported to a spreadsheet program (Microsoft Excel).

Temporal Profile Data Analysis—Data analysis was performed in R (cran.r-project.org). For data normalization, the spot intensity vectors per time point were first scaled to a constant sum of intensities, and then the time series vector per spot was rescaled so that the maximum intensity was standardized to a value of 1,000. Spots were classified into groups with similar time profiles with the partitioning around medoids (PAM) algorithm (46) and a predefined number of 24 groups because silhouette width values did not support any specific number of groups in the data. Details about the choice of this value of 24 is available in the supplemental information. Only the 898 spots that were found in at least two time points were used. Of the 490 spots detected at only one time point, only one representative from each of the six time points was taken for analysis. The distance measure was 1 − Pearson correlation for the transformed variable $Z = \log_2$ (1 + ratio of the intensity to the mean intensity). Color-coded intensity plots for Z were produced with the function "heatmap." Relationships between the 24 groups were visualized in a hierarchical clustering dendrogram of their average profiles (hclust function in R, average linkage method, 1 − Pearson correlation as distance). For cross-correlation analysis, the pairwise Pearson correlations were computed between each of the averaged profiles of the 24 groups, and this correlation matrix was represented on a false color scale.

Flow Cytometry-based Uptake Assay—We used a flow cytometry-based particle uptake assay detailed in the supplemental information. Briefly 10^7 cells grown on plates were harvested, resuspended in 5 ml of HL5c medium, placed in one well of a 6-well plate, and shaken at 150 rpm. After washing, 2×10^9 1-μm fluorescent beads (Fluoresbrite YG 1-μm microspheres, Polysciences, Inc.) were added to the cells in suspension and incubated at room temperature under constant shaking at 120 rpm. At each time point, 0.5 ml of cells was harvested, and bead uptake was stopped. Then cells were centrifuged at 500 × *g* for 5 min at 4 °C, resuspended in 0.5 ml of ice-cold Soerensen buffer containing 120 mM sorbitol, and kept on ice until fluorescence-activated cell sorter data acquisition. For each time point, 30,000 fluorescence events were acquired using a FACScan flow cytometer (BD Biosciences), and bead uptake was quantified. Mean fluorescence was calculated by analyzing histograms showing fluorescence *versus* events. Supplemental information is available.

RESULTS AND DISCUSSION

In analyzing the proteome of *Dictyostelium* phagosomes, we had two aims: to identify new protein components and to see how phagosome proteins change during maturation. To do so, we prepared large amounts of latex bead phagosomes by using a protocol that includes physiological concentrations of ATP, ensuring high yields and purity (see supplemental information). Briefly using markers for a variety of organelles, we calculated that our phagosome fractions were enriched up to about 100-fold over a crude membrane fraction and were depleted about 10-fold of major contaminants, such as contractile vacuole, endoplasmic reticulum, and mitochondria (16, 35). In addition, our pulse-chase protocol allows purification of phagosome at various times that were shown previously to cover all the steps of *Dictyostelium* phagosome maturation from uptake through digestion and finally to exocytosis of the undigested remnants (16). We separated phagosome proteins by 2D gel electrophoresis using preparative gels from which we picked spots and identified the corresponding proteins (Fig. 1) and analytical gels of six different time points during maturation from which we computed a time profile for each spot (Figs. 2 and 3).

Identification of Phagosome Proteins—We began by applying standard protein extraction, solubilization, and 2D gel procedures (see "Experimental Procedures") to analyze the prepared phagosomes. This resulted in highly reproducible gels with very good spot quality (see for example, Fig. 1*A* (gel A); see also Ref. 16). However, because these procedures do not solubilize hydrophobic and transmembrane proteins very well, we also explored a variety of the latest generation detergents (see supplemental information) as well as various extraction methods and 2D gel protocols. Carbonate extraction (36) followed by solubilization in a buffer containing 2% CHAPS and 2% 4-octylbenzoylamidopropyldimethylammoniopropanesulfonate (47) yielded excellent results; a preparative gel (gel B) from a phagosome extract prepared according to this method is shown in Fig. 1*B*.

A total of 180 and 232 spots were picked from gels A and B, respectively, and analyzed by peptide fingerprinting (see "Experimental Procedures" and Supplemental Figs. S1 and S2 for spectra). Among these, 11 spots were keratin, and 72 others could not be identified for technical reasons. In addition, four proteins corresponding to spots 134 and 135 of gel A and spots 136 and 166 of gel B were identified by ESI-MS/MS (see Supplemental Table SI and Figs. S1 and S2 for representative spectra). In total, 137 spots from gel A and 192 spots from gel B were identified as known proteins or predicted open reading frames in the *Dictyostelium* genome (dictybase.org (12)). Taking into account the proteins common to both gels and counting proteins present as multiple spots, including degradation products, as one protein, a total of 179 different proteins were finally identified. Table I lists all these

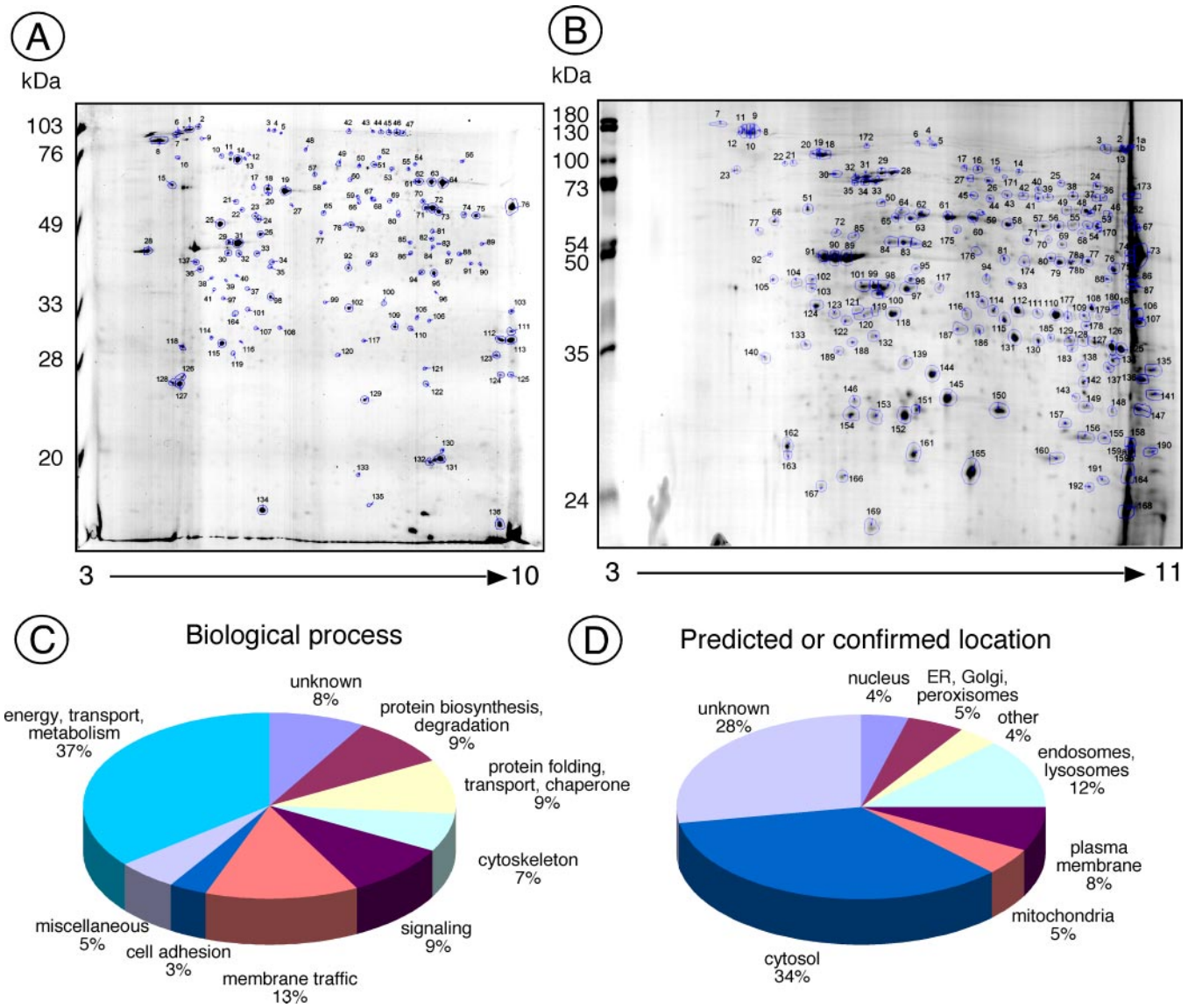

FIG. 1. **2D gel electrophoresis of phagosome proteins, their predicted functions, and subcellular locations.** Preparative 2D gels of phagosome proteins extracted under standard conditions (*A*) or under conditions that favor extraction of membrane proteins (*B*) are shown. The phagosomes analyzed in gel A are a pool of the early three time points of a pulse-chase feeding (see Fig. 2), whereas gel B is derived from a pool from the three late time points. The pH range of the first dimension isoelectric focusing gel is shown at the *bottom*, and the sizes of molecular mass standards for the second dimension are indicated on the *left* in kDa. The proteins corresponding to 137 spots on gel A and 192 spots on gel B (*circled* in *blue*) were identified by mass spectrometry and comparison with the *Dictyostelium* genome. Further data are compiled in Table I and Supplemental Table SI. The identified phagosomal proteins were classified according to their predicted or known functions (*C*) and subcellular locations (*D*).

proteins, their location(s) on each gel, their known or proposed functions and cellular locations, whether they were found previously in the mouse phagosome proteome (11), and whether their presence has been confirmed by our ongoing large scale analysis of *Dictyostelium* phagosomes by one-dimensional gel electrophoresis and liquid chromatography tandem mass spectrometry.[2] Supplemental Table SI presents additional basic information about each spot identification.

The phagosomal proteins we identified belonged to a variety of functional classes (Fig. 1*C*). Reflecting the digestive character of phagosomes and their export of nutrients to the cytosol, 37% of the proteins were members of the "energy, transport, and metabolism" class. The second largest group, comprising 13% of polypeptides, was proteins involved in membrane traffic, reflecting the importance of transport to and from the maturing phagosome. Among them, we found a large collection of small GTPases, some of which are known

[2] M. Desjardins, M. Hagedorn, R. Dieckmann, and T. Soldati, unpublished data.

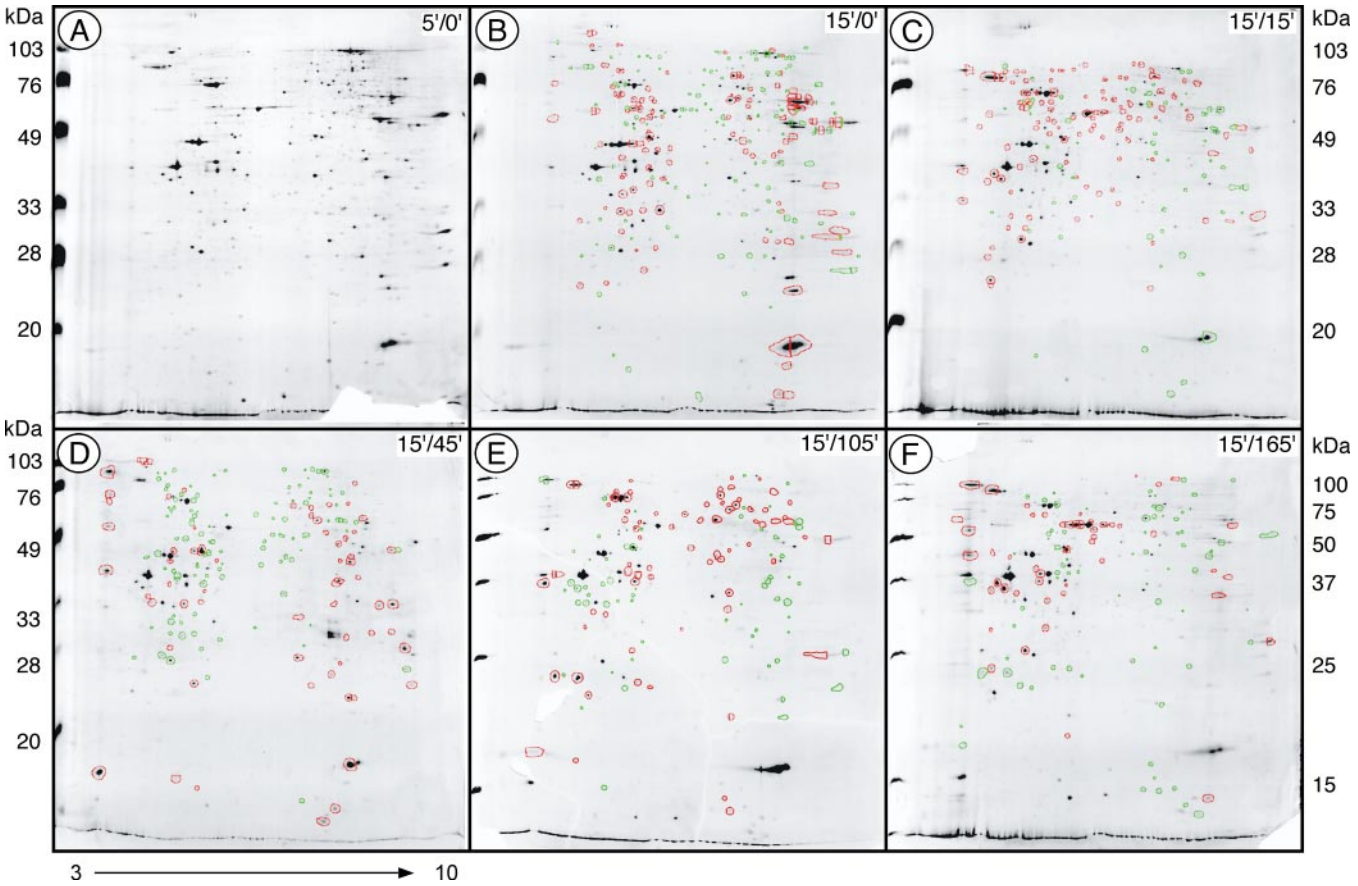

FIG. 2. **Changes in protein composition accompanying phagosome maturation.** 2D gels of phagosomal proteins purified at six time points during a pulse-chase feeding regime as indicated at the *top right corner* of each gel are shown. With the exception of spots that completely disappear or appear (see Table III) the spots that are at least 2-fold more abundant than at the previous time point (*e.g.* in *B* compared with *A*) are *circled* in *red*; spots that are at least 2-fold less abundant are *circled* in *green*. *B* shows 116 *red* and 128 *green* spots; *C* shows 111 red and 65 green spots; *D* shows 65 *red* and 105 *green* spots; *E* shows 74 *red* and 63 *green* spots; *F* shows 49 *red* and 72 *green* spots. Labeling of the gels is as in Fig. 1.

to play a role in uptake processes in *Dictyostelium* (24, 48–50) and macrophages (51, 52). Of these, Rab11B, Rab14, Rab7, and Rap1 were also found in mouse phagosomes (11), and Rab7 was found in *E. histolytica* phagosomes (31), indicating that the phagocytic mechanisms have been conserved through evolution. In the membrane traffic group, we also detected members of the SNARE machinery responsible for the specificity of membrane fusion. Of these, only α- and γ-SNAP (soluble NSF attachment protein) have been found in mouse phagosomes. We also found dynamin, a protein involved in vesicle fission.

Other large groups of proteins we identified function in signal transduction (9%) and cytoskeleton organization (7%). These signaling proteins included the heterotrimeric G protein subunits Gβ, another Gβ-like protein, and Gα_4. Gα_2, Gβ_1, and Gβ_2 have been found previously in mouse phagosomes (11). Not surprisingly, in view of their richly documented role in phagocytosis, we found a large variety of cytoskeleton proteins, some of which have also been found in mouse phagosomes. In addition to the signaling and cytoskeleton functional groups, we found a large group of heat shock proteins (HSPs) and other chaperones (9% of all proteins). HSPs act as chaperones and assist protein synthesis, folding, and breakdown. They also regulate actin polymerization/capping, uncoating of clathrin-coated vesicles, and phagocytosis in macrophages (53). Besides proteins known to play a role in phagocytosis and known proteins for which a role in phagocytosis has not been described, the functions of over 35 conserved proteins we identified (8%) are not known. Additional research will be necessary to assess the role of these novel candidates in phagocytic functions.

Fig. 1*D* shows the known or predicted subcellular locations of the phagosome components we identified. Cytosolic proteins comprise 34%, endosomal and lysosomal proteins comprise 12%, and plasma membrane proteins comprise 8% of the total. The subcellular locations of 28% of them, however, are not known. This broad variety of functions and subcellular locations reflects the complex processes involved in the uptake of particles and the subsequent maturation of the phagosome into a killing and digestive compartment. It is impor-

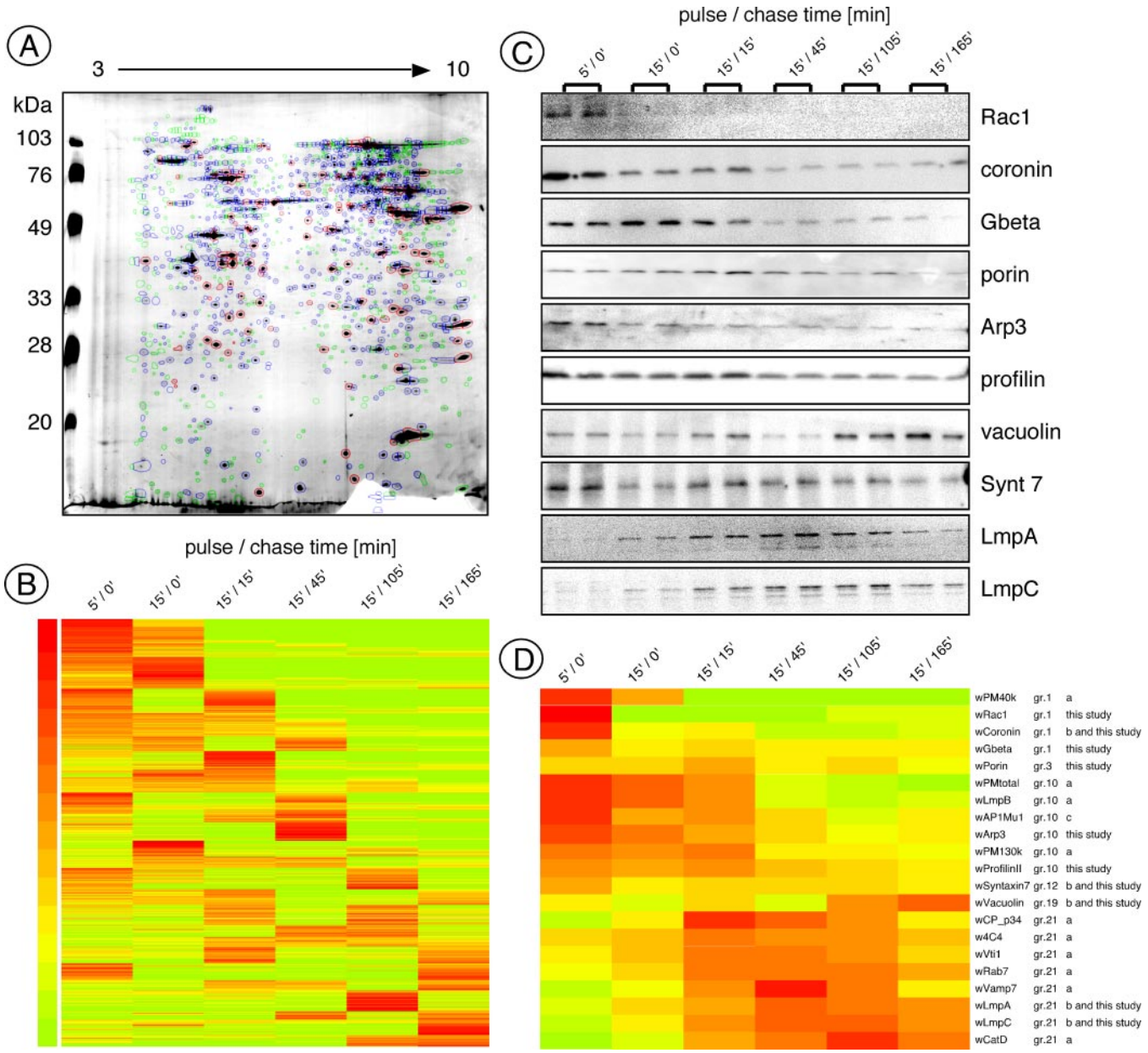

FIG. 3. **Temporal profiling of phagosome proteins by 2D gel and Western blotting.** *A*, a composite image of a 2D gel in which all 1,388 spots from the six time points in Fig. 2 have been superimposed on the gel from time point 5′/0′. The 490 spots present at a single time point are *circled* in *green*; the 125 spots matched to spots identified on the two preparative gels are *circled* in *red*. The remaining 773 spots are *circled* in *blue*. Labeling of the gels is as in Fig. 1. *B*, a heat map showing the computed and normalized intensities of 904 spots over the six time points, including the 898 spots present at two or more time points and the six representative spots present at a single time point. *C*, Western blotting of a selection of 21 endosomal/phagosomal proteins over the time course of phagocytosis. Only the 10 previously unpublished blots are shown. *D*, a heat map derived from the quantitative data produced by densitometry of the 21 blots, obtained from the various experiments indicated on the *right*: "*a*," blots and profiles published in Ref. 16; "*b*," profiles but not blots published in Ref. 16; "*c*," blot and profile published in Ref. 68. The "*w*" (also used in Supplemental Figs. S3-1 to S3-6) indicates that these profiles were obtained from Western blotting.

tant to note that it is difficult to judge *a priori* the specificity of the presence of cytosolic proteins on phagosomes. As detailed in the supplemental information, some abundant cytosolic proteins are represented, but many are not. In addition, the fact that the presence of most proteins follows a complex temporal profile speaks against a simple piggy-backing during purification but in favor of a specific and regulated recruitment.

Many of the proteins we identified have evident roles to play at one or another stage of phagosome maturation (see above), but the presence of others is more surprising and might reveal additional processes linked to the phagosome.

TABLE I

Proteins identified from preparative gels

This table lists the 179 proteins identified after picking spots highlighted on gels A and B in Fig. 1.

Spot GelA	Spot GelB	Gene name	Gene product	Biological Process	Molecular function	Predicted location	Group	LC-MS/MS	Found in mouse phagosome	Comment
80	74	serA	3-phosphoglycerate dehydrogenase (PHGDH)	serine biosynthesis / metabolism	oxidoreductase activity	cytosolic	10	X		
101		rpsA	40S ribosomal protein SA	protein biosynthesis	structural constituent of ribosome	cytosolic / endoplasmic reticulum	8	X	X (Rsp4)	ER-associated ?
105	107	RPLP0	60S acidic ribosomal protein P0	protein biosynthesis	structural constituent of ribosome	cytosolic / endoplasmic reticulum	12	X	X (Rsp4)	ER-associated ?
	190	rpl9	60S ribosomal protein L9	protein biosynthesis	structural constituent of ribosome	cytosolic / endoplasmic reticulum		X	X (Rsp4)	ER-associated ?
21		argE	Acetylornithine deacetylase	arginine biosynthesis / metabolism	metallopeptidase activity	cytosolic	11			
	121	act23	Actin 23	cytoskeleton	structural constituent of cytoskeleton	cytosolic				
25, 32, 39, 40, 97, 104	89, 90, 91, 95, 100, 106, 117, 119, 132	act	Actin(s) different genes same match	cytoskeleton	structural constituent of cytoskeleton	cytosolic	15	X	X	found in exosomes
65		sahA	Adenosylhomocysteinase	one-carbon compound metabolism	adenosylhomocysteinase activity	cytosolic	15			found in actin rods
81		purA	Adenylosuccinate synthetase	purine nucleotide biosynthesis	adenylosuccinate synthase activity	cytosolic				
	93	DDB0203373	AgCP2753 (Fragment)	aromatic amino acid family metabolism	4-hydroxyphenylpyruvate dioxygenase activity	cytosolic				
122		pefA	ALG-2A (or Pef1, penta-EF-hand Ca2+-binding protein)	signalling / membrane traffic	calcium ion binding	cytosolic / endosomal	7	X		endosomal protein sorting ?
	63, 65, 182	tubA	Alpha tubulin	cytoskeleton	structural constituent of cytoskeleton			X	X	found in exosomes
73		anxA	Annexin VII	signalling / membrane traffic	rhodopsin-like receptor activity	membrane	2		X (annexin5)	found in exosomes
	165	arfA	Arf1 GTPase	membrane traffic	GTP binding	cytosolic		X		ER Golgi ?
	175	actA	Arp3	cytoskeleton	structural constituent of cytoskeleton	cytosolic		X	X	actin nucleation
	104	arsA	Arsenite-translocating ATPase	transport	arsenite-transporting ATPase activity	membrane		X		
	42	asnA	Asparagine synthetase	metabolism	asparagine synthase (glutamine-hydrolyzing) activity	cytosolic				
	171	asnS1	Asparaginyl-tRNA synthetase	asparaginyl-tRNA aminoacylation	asparagine-tRNA ligase activity	cytosolic				
	54, 57	pyr56	Bifunctional UMP-synthetase	pyrimidine nucleotide biosynthesis	orotidine-5'-phosphate decarboxylase activity	unknown				
	167	cbpM	Calcium-binding protein (NCS-1/frequenin-related protein)	unknown	calcium ion binding	unknown				
115	146	cadA	Calcium-dependent cell adhesion molecule-1	cell-cell adhesion	protein homodimerization activity	plasma membrane	15	X		
15	66	crtA	Calreticulin	chaperone	calcium ion binding	endoplasmic reticulum	14	X	X	ER fusion with phagosomes ?
	7	GP138A	Cell surface glycoprotein gp138	cell-cell adhesion	unknown	plasma membrane		X		
	166	coaA	Coactosin	cytoskeleton	actin binding	cytosolic		X		
	161	cofA	Cofilin	cytoskeleton	actin monomer binding	cytosolic		X		actin filament depolymerization
124, 125, 136		comA	Comitin	membrane traffic	sugar binding	Golgi membrane	12	X		reported to bind actin
59		corA	Coronin	cytoskeleton	actin binding	cytosolic	11		X	
	70	ctxA	Cortexillin I	cytoskeleton	actin binding	cytosolic				cellular morphogenesis
99	131, 186, 187	discA	Discoidin I, alpha chain	cell adhesion	unknown	plasma membrane	15	X		
100	125, 127, 129	discB	Discoidin I, beta or gamma chain	cell adhesion	unknown	plasma membrane	12			
	126, 128, 184	discD	Discoidin I, D chain	cell adhesion	unknown	plasma membrane				
109		discE	Discoidin II	cell adhesion	unknown	plasma membrane	11	X		
47, 49, 60	1a, 2, 3, 41, 43, 56	dymA	Dynamin	membrane traffic	GTP binding	cytosolic / endosomal	1	X		at the crossroads of actin dynamics and membrane traffic
	85	flhB	Flavohemoglobin	electron transport	oxidoreductase activity	unknown				
48	16, 17	glnB	Glutamine synthetase, type III	nitrogen compound metabolism	glutamate-ammonia ligase activity	unknown	18			
85		gpdA	Glyceraldehyde-3-phosphate dehydrogenase (GAPDH)	glucose metabolism	glyceraldehyde-3-phosphate dehydrogenase activity	cytosolic / mitochondrial	13	X	X	found in exosomes
	14, 15	guaA	GMP synthetase	purine nucleotide biosynthesis	GMP synthase (glutamine-hydrolyzing) activity	unknown				
	134	gchA	GTP cyclohydrolase I	tetrahydrobiopterin biosynthesis	GTP cyclohydrolase I activity	cytosolic				
110		hspB/hspE	Heat shock cognate protein 70 kD (hsc70 or hsc70-2)	chaperone	agonist-regulated F-actin capping activity	cytosolic	10		X	found in exosomes
11	31, 32	hspB	Heat shock cognate protein 70 kD (hsc70)	chaperone	agonist-regulated F-actin capping activity	cytosolic	11	X	X	found in exosomes
12, 108	28, 29	hspE	Heat shock cognate protein 70 kD (Hsc70-2)	chaperone	agonist-regulated F-actin capping activity	cytosolic	11	X	X	found in exosomes
9	18, 19, 20	hspD	Heat shock cognate protein 90 kD (hsc90)	chaperone	ATP binding	cytosolic	3	X	X	found in exosomes
	172	hspH	Heat shock protein 88kDa	chaperone	ATP binding	cytosolic				
71, 72, 94, 102	75	ddj1	Heat shock protein Ddj1	chaperone	protein folding	cytosolic	13	X		
87		gpaD	Heterotrimeric G-protein subunit alpha 4	G-protein coupled receptor protein signaling pathway	signal transducer activity	plasma membrane	8		X (Galpha2 subunit)	found in exosomes
93, 98, 126	108	gpbA	Heterotrimeric G-protein subunit beta	G-protein coupled receptor protein signaling pathway	signal transducer activity	plasma membrane	13	X	X (Gbeta1,2 subunits)	found in exosomes
95		DDB0185122	Heterotrimeric G-protein subunit beta-like	G-protein coupled receptor protein signaling pathway	signal transducer activity	plasma membrane	12	X		
132	168	hatA	Hisactophilin 1	cytoskeleton	pH-sensitive actin-binding	cytosolic	4			
131		hatB	Hisactophilin 2	cytoskeleton	pH-sensitive actin-binding	cytosolic	2			
77	81	ifdA	IfdA (Similar to ATP-dependent, RNA helicase)	unknown	ATP-dependent helicase activity	unknown	9	X		
61		purH	IMP cyclohydrolase	purine nucleotide biosynthesis	IMP cyclohydrolase activity	cytosolic	11	X		
	50	lrrA	Leucine-rich-repeat protein A	unknown	unknown	unknown		X		
	8, 9, 10, 11, 12	gp130	Lipid-anchored plasma membrane glycoprotein 130	membrane traffic	unknown	plasma membrane		X		
	25	fetA	Long-chain fatty acyl-CoA synthetase	fatty acid metabolism	long-chain-fatty-acid-CoA ligase activity	endosomal		X		
	45	lysS	Lysyl tRNA Synthetase	lysyl-tRNA aminoacylation	lysine-tRNA ligase activity	cytosolic				
42		mvpA	Major vault protein alpha	unknown	unknown	cytosolic	3			
3, 4	4	mvpB	Major Vault Protein beta	unknown	unknown	cytosolic	10	X		
	135	porA	Mitochondrial porin	transport	voltage-gated ion-selective channel activity	mitochondrial / plasma membrane		X	X	
28		DidioMp37	NADH ubiquinone oxidoreductase 80 kDa subunit	metabolism	oxidoreductase activity	unknown	19			
90		nek2	Nek (NimA-related) family protein kinase	regulation of cell cycle	protein serine/threonine kinase activity	cytosolic	4			
130		ndkC	Nucleoside diphosphate kinase (NDPK)	metabolism	nucleoside-diphosphate kinase activity	cytosolic			X	found on mammalian phagosomes
	77	pctA	Phosphoethanolamine-cytidyltransferase	metabolism	involved in sphingomyelin degradation pathway	unknown				lipid remodeling?
	58	pgkA	Phosphoglycerate kinase	glucose metabolism	phosphoglycerate kinase activity	cytosol				
	138	gpmA	Phosphoglycerate mutase	glucose metabolism	phosphoglycerate mutase activity	cytosolic				found in exosomes
135		pkiA	PKIA (similar to protein kinase C inhibitor)	signalling	unknown	cytoplasm	13	X		
91		disA	Protein disulfide isomerase	protein folding / chaperone	isomerase activity	endoplasmic reticulum	12	X	X (P5 type)	ER fusion ?
	68	DDB0168337	Putative 26S proteasome regulatory particle triple-A ATPase subunit1	proteolysis and peptidolysis	hydrolase activity	cytosolic				
	44	DDB0202018	Putative 26S proteasome subunit 4	proteolysis and peptidolysis	hydrolase activity	cytosolic				
133		rps12	Putative 40S ribosomal protein S12	protein biosynthesis	structural constituent of ribosome	cytosolic	13	X		
	30	DDB0167089	Putative 78 kDa glucose-regulated protein homolog precursor	chaperone	ATP binding	endoplasmic reticulum		X		ER fusion ?
	37	DDB0230064	Putative adenylylsulfate kinase	methionine metabolism	sulfate adenylyltransferase (ATP) activity	cytosolic				
	114	DDB0169112	Putative aldehyde reductase	metabolism	reductase	unknown				
68	53, 55	DDB0205386	Putative ATP citrate lyase b-subunit	citrate metabolism	ATP citrate synthase activity	mitochondrial	18			found in exosomes
	183	DDB0184316	Putative ATP synthase F1 subunit alpha	ATP synthesis coupled proton	hydrogen-transporting ATPase	mitochondrial		X	X (beta subunit)	
	59	DDB0183841	Putative CCT chaperonin beta subunit	chaperone	protein folding	cytosolic				
	46	DDB0204641	Putative CCT chaperonin gamma subunit	chaperone	protein folding	cytosolic				
	48, 49, 109	DDB0169209	Putative chaperonin containing TCP-1 zeta subunit	chaperone	protein folding	cytosolic		X		
	78b	DDB0167789	Putative chromosome segregation ATPase	cell cycle regulation	ATPase	unknown		X		
82, 83	86, 87	CnrD	Putative countin receptor Cnr4 (Cue domain, involved in binding ubiquitin-conjugating enzymes)	signalling	unknown	unknown / membrane	15			
	76, 78a	DDB0231401	Putative cytosolic NADP-dependent isocitrate dehydrogenase	metabolism	dehydrogenase	cytosolic				
	176	DDB0169465	Putative decarboxylase	polyamine biosynthesis	decarboxylase	unknown				
	143	DDB0168923	Putative dihydropteridine reductase	metabolism	oxidoreductase activity	unknown				
	180	DDB0204015	Putative D-lactate dehydrogenase	serine biosynthesis	oxidoreductase activity	unknown				found in exosomes
	82	DDB0185297	Putative eucaryotic translation elongation factor 1 gamma	protein biosynthesis	translation elongation factor activity	cytosolic				reported to bind actin
	148	DDB0231431	Putative glutathione S-transferase	metabolism	glutathione S-transferase	unknown				found in exosomes
	151	DDB0217453	Putative glutathione S-transferase	metabolism	glutathione S-transferase	unknown				found in exosomes
	26, 27	glyS	Putative glycyl-tRNA synthetase	glycyl-tRNA aminoacylation	glycine-tRNA ligase activity	cytosolic				
	122	DDB0185935	Putative inorganic pyrophosphatase	metabolism	pyrophosphatase	unknown				
	102	DDB0203989	Putative ketol-acid reductoisomerase	metabolism	reductoisomerase	unknown				
	71	DDB0189202	Putative mitochondrial processing peptidase alpha subunit	protein import	peptidase	mitochondrial		X		
	72	DDB0188097	Putative mitochondrial processing peptidase beta subunit	protein import	peptidase	mitochondrial		X		
107	139	DDB0229909	Putative O-methyltransferase	metabolism	O-methyltransferase activity	unknown	11			
23	83, 84	DDB0185641	Putative oxysterol-binding protein (OSBPL7)	membrane traffic	oxysterol binding	membrane	22	X		
	192	DDB0218719	Putative peroxiredoxin	metabolism	oxidoreductase activity	unknown				
	47	DDB0205849	Putative peroxisomal-coenzyme A synthetase	metabolism	AMP binding	peroxisomal				
	36	DDB0231108	Putative phosphoenolpyruvate carboxykinase	metabolism	phosphoenolpyruvate carboxykinase activity	cytosolic				
	173	DDB0192007	Putative poly(A)-mRNA binding protein	gene expression	RNA binding	cytosolic / nuclear		X		
	157	DDB0219666	Putative prenylated SNARE protein Ykt6	membrane traffic	membrane fusion	endosomal		X		
27		DDB0218402	Putative RNA 3'-terminal phosphate cyclase-like protein	gene expression	cyclase	unknown	6			
	88	DDB0201846	Putative RNA binding protein NAPOR-3	gene expression	RNA binding	nuclear		X		
	188	DDB0187734	Putative SAM-dependent methyltransferase	metabolism	methyl transferase	unknown				
69		DDB0230072	Putative serine hydroxymethyltransferase	metabolism	methyl transferase	cytosolic	13			
	67	DDB0167129	Putative signal recognition particle 54 kDa protein	protein biosynthesis	RNA binding	cytosolic		X		
	69	DDB0217073	Putative sorting nexin 2	membrane traffic	lipid binding	endosomal		X		
	115, 116	DDB0187880	Putative stress induced pyridoxin biosynthesis PDX1-like protein SOR1	metabolism	pyridoxin biosynthesis	unknown				

TABLE I—*continued*

Spot GelA	Spot GelB	Gene name	Gene product	Biological Process	Molecular function	Predicted location	Group	LC-MS/MS	Found in mouse phagosome	Comment
70		DDB0189391	Putative synaptosomal-associated protein (SNAP25, GRAM domain, t-SNARE coiled-coil homology domain)	membrane traffic	membrane fusion	plasma membrane	12	X		ER fusion ?
106				ATP synthesis coupled proton transport	hydrogen-transporting ATP synthase	endosomal / mitochondria	9	X		
57		DDB0167892 DDB0188782	Putative vacuolar ATP synthase subunit D Putative vacuolar protein sorting-associated protein 45 (vps45)	membrane traffic	unknown	endosomal	6			
	137	pdhA	Pyruvate dehydrogenase E1 alpha subunit	metabolism	oxidoreductase activity	unknown				
129	145	rab11A	Rab11A GTPase	membrane traffic	GTP binding	endosomal	19	X	X (Rab11B)	
	144	rab11C	Rab11C GTPase	membrane traffic	GTP binding	endosomal			X (Rab11B)	
	155, 158, 159b	rab14	Rab14 GTPase	membrane traffic	GTP binding	endosomal			X	
	150	rab1D	Rab1D GTPase	membrane traffic	GTP binding	Golgi membrane		X		
	149, 191	rab32A	Rab32A GTPase	membrane traffic	GTP binding	endosomal		X		
	156	rab7A	Rab7A GTPase	membrane traffic	GTP binding	endosomal		X	X	
	159a	rac1A	Rac1A GTPase	signalling	GTP binding	plasma membrane		X		
	133	DDB0187464	Ran-specific GTPase-activating protein	protein transport	GTPase activating	cytosolic				
	160	rapA	Rap1 GTPase	signalling	GTP binding	plasma membrane / endosomal		X	X	
	154	rasB	RasB GTPase	signalling	GTP binding	plasma membrane / endosomal		X		
	152, 153	rasG	RasG GTPase	signalling	GTP binding	plasma membrane / endosomal		X		reported to modulate actin dynamics
	92	rcbA	Rep-C binding protein A	nucleotide-excision repair	nucleotide-excision repair	nuclear				
88		DDB0185717	RNA Export 1 homolog or AGL301Cp	RNA transport	RNA binding	nuclear	1	X		
79	79, 174	DDB0230070	S-adenosylmethionine synthetase	methionine metabolism	methionine adenosyltransferase activity	cytosolic	1	X		
	164	sar1A	Sar1 GTPase	membrane traffic	GTP binding	endoplasmic reticulum		X		ER fusion ?
	170	serS	SeryI-tRNA aminoacylation	seryl-tRNA aminoacylation	serine-tRNA ligase activity	cytosolic				
84		sevA	Severin	cytoskeleton	actin severing	cytosolic	7	X		
96		DDB0186131	Similar to ribose-phosphate pyrophosphokinase	metabolism	pyrophosphokinase	unknown	7			
38	123	snpA	Soluble NSF attachment protein alpha isoform	membrane traffic	membrane fusion	cytosolic	21		X	
34		snpC	Soluble NSF attachment protein gamma isoform	membrane traffic	membrane fusion	cytosolic	1	X	X	
52		tkt	Transketolase, glycolaldehydetransferase	metabolism	transferase	cytosol	11			
	140	efa1B	Translation elongation factor 1 beta	protein biosynthesis	translation elongation factor activity	cytosolic		X		reported to bind actin
43, 44, 45, 46, 66	1b, 13	efhA	Translation elongation factor 2	protein biosynthesis	translation elongation factor activity	cytosolic	10	X		reported to bind actin / found in exosomes
74, 75, 76	73	efaAII	Translation elongation factor eEF-1 alpha chain	protein biosynthesis	translation elongation factor activity	cytosolic	12	X	X	reported to bind actin
	51	sonA	Ubiquitin-like fusion protein SonA; suppressor of NosA	signalling	unknown	unknown		X		
10		DDB0190669	Unknown (ATP synthase beta-subunit)	ATP synthesis coupled proton transport	hydrogen-transporting ATP synthase	mitochondrial	20	X		
16		DDB0202870	Unknown (C2 calcium/lipid-binding region, CaLB)	unknown	unknown	unknown	14			
86		DDB0167100	Unknown (conserved hypothetical protein dTDP-glucose 4,6-dehydratase Entamoeba histolytica, epimerase)	metabolism	epimerase	cytoplasmic	12	X		
67		DDB0185844	Unknown (no significant BLAST hit)	unknown	unknown	unknown	16			
8		DDB0186893	Unknown (no significant BLAST hit)	unknown	unknown	unknown	17	X		
	105	DDB0189279	Unknown (RNA or DNA binding domain)	unknown	RNA binding	unknown		X		
	189	DDB0169073	Unknown (similar to ATP synthase F0 D chain)	ATP synthesis coupled proton transport	hydrogen-transporting ATP synthase	mitochondrial		X		
58		DDB0186598	Unknown (similar to cell division cycle 20 homolog S. cerevisiae)	cell cycle regulation	kinase	nuclear / cytosol	9	X		
	21, 22	DDB0203503	Unknown (similar to COG5651: PPE-repeat proteins Chloroflexus aurantiacus)	unknown	unknown	unknown				
	181	DDB0219824	Unknown (similar to CSN complex subunit 6A, COP9 signalosome)	signalling	unknown	unknown				
1, 2, 6, 7		DDB0217534	Unknown (similar to Entamoeba histolytica, myosin heavy chain)	unknown	unknown	unknown	10			
50	38, 39	DDB0185738	Unknown (similar to formyltetrahydrofolate deformylase PurU Helicobacter hepaticus)	metabolism	deformylase	membrane	7	X		
134		DDB0204332	Unknown (similar to HLA-B associated transcript 1; DEAD-box nuclear RNA helicase Pan troglodytes)	gene expression	RNA helicase	nuclear	6	X		
22		DDB0167836	Unknown (similar to human tumor-suppressing SUBCHROMOSOMAL TRANSFERABLE fragment 1, WD-40 repeat)	unknown	unknown	unknown	14			
5	5, 6	DDB0205268	Unknown (similar to hypothetical protein (sec23/24 trunk domain))	unknown	unknown	cytosolic		X		
117	141, 142	DDB0215963	Unknown (similar to imidazoleglycerol-phosphate synthase subunit H-like Arabidopsis thaliana)	metabolism	SNO glutamine amidotransferase	unknown	4	X		
	177	DDB0184451	Unknown (similar to Lactococcus lactis oxidoreductase)	metabolism	oxidoreductase	unknown				
78	80	DDB0188543	Unknown (similar to late embryonic abundant protein EMB8 - white spruce, hydrolase or acyltransferase)	metabolism	abhydrolase	unknown	22	X		
	179	DDB0187193	Unknown (similar to Mung bean, aldehyde reductase, C2 domain)	metabolism	epimerase	unknown				
120		DDB0217516	Unknown (similar to Peroxiredoxin 4)	metabolism	oxidoreductase	unknown	13			
	23	DDB0204691	Unknown (similar to probable glycosyl hydrolase Pseudomonas aeruginosa)	metabolism	glycosyl hydrolase	membrane		X		
35		DDB0204870	Unknown (similar to Proteasome inhibitor PI31 subunit (hPI31), partial (Gallus gallus)	proteolysis and peptidolysis	unknown	unknown	7			
121		DDB0189483	Unknown (similar to protein kinase, lysine deficient 4 Canis familiaris)	signalling	kinase ?	unknown				
62, 63, 64, 89	52	DDB0219363	Unknown (similar to Q99615 DnaJ homolog subfamily C member 7 (Tetratricopeptide repeat protein 2))	chaperone	unknown	unknown	18	X		
92	110, 111, 112, 113, 178, 185	DDB0188166	Unknown (similar to S-adenosyl-methionine cyclouartenol-C 24-methyltransferase)	metabolism	methyltransferase	unknown	18	X		
37	118, 120	DDB0202301	Unknown (similar to SAM-dependent methyltransferases Pseudomonas aeruginosa)	metabolism	methyltransferase	unknown	11	X		
118		DDB0217461	Unknown (similar to SET and MYND domain Rattus norvegicus)	unknown	unknown	unknown	14			
	130	DDB0219578	Unknown (similar to short-chain alcohol dehydrogenases Methylobacillus flagellatus)	metabolism	dehydrogenase	unknown				
103		DDB0192039	Unknown (similar to short-chain dehydrogenase/reductase (SDR) family protein Arabidopsis thaliana)	metabolism	dehydrogenase	nuclear		X		
137	124	DDB0206532	Unknown (similar to small glutamine-rich protein containing three tetratricopeptide repeats Apis mellifera)	cochaperone	interaction with the ubiquitin-dependent endocytosis motif	unknown	16	X		
	169	DDB0188978	Unknown (similar to src homology 3 domain-containing protein HIP-55 Apis mellifera, ADF domain)	membrane traffic / cytoskeleton	unknown	endosomal / cytosolic				
	40	DDB0184362	Unknown (similar to stress-induced protein sti1-like protein)	signalling	unknown	unknown				
56		DDB0190403	Unknown (similar to stress-induced-phosphoprotein 1 like Caenorhabditis elegans, Zinc finger, C3HC4 type (RING finger) Tetratricopeptide repeat)	signalling	unknown	unknown	1			
123	147	DDB0204139	Unknown (similar to Tat-interacting protein Tip30 Danio rerio)	unknown	unknown	unknown	23	X		
119		DDB0168691	Unknown (similar to Zgc:100982 protein Danio rerio hippocalcin-like 1, EF-hand)	signalling	calcium ion binding	unknown	10	X		
54		DDB0205389	Unknown (similar to ATP citrate-lyase)	metabolism	unknown	cytosolic / membrane	12			
	94	hemE	Uroporphyrinogen decarboxylase	metabolism	decarboxylase	unknown				
26, 29, 30, 31, 36, 41, 127, 128	96, 99, 101, 162, 163	vatM	Vacuolar H+-ATPase 100-kDa subunit	proton transport	proton channel	endosomal	19	X		
13, 14, 24, 114	33, 34, 35	vatA	Vacuolar H+-ATPase A subunit	proton transport	ATPase	endosomal	15	X	X	
17, 18, 19, 20, 116	60, 61, 62, 64	vatB	Vacuolar H+-ATPase B subunit	proton transport	ATPase	endosomal	11	X	X	
	103	vatD	Vacuolar H+-ATPase D subunit	proton transport	ATPase	endosomal		X		
111, 112, 113	136	vatE	Vacuolar H+-ATPase E subunit	proton transport	ATPase	endosomal		X	X	
51, 53	24	vacA1	Vacuolin A	membrane traffic	unknown	endosomal	19	X		
55		vacB	Vacuolin B	membrane traffic	unknown	endosomal	15	X		
33	97, 98	DDB0187546	Vegetative Specific Protein H5 (esterase/lipase domain)	metabolism	esterase	unknown	5	X		

One such example is the identification of proteins from the ER, Golgi apparatus, and peroxisomes among the phagosome proteins. The presence of four ribosomal components, four tRNA synthetases, the 54-kDa subunit of the signal recognition particle, and three translation elongation factors (which are actin-binding proteins), all factors involved in protein biosynthesis, may be explained either by protein synthesis taking place on the phagosome itself or substantial association/fusion of phagosomes with the ER (54). This latter hypothesis is supported by the presence of a subset of ER-resident proteins (calreticulin, protein-disulfide isomerase, and a homologue of the immunoglobulin Binding Protein BiP) and ER export/trafficking regulators (Sar1 and Rab1D) in the phagosomes.

Dynamics of the Phagosome Proteome—To generate temporal profiles of phagosome proteins during maturation, we made use of our established pulse-chase protocol (see supplemental information). For each maturation stage we quan-

TABLE II
Statistics of detection of protein spots

Time point	Not detected	Detected	At peak	Percentage at peak	Specific for this time	Percentage specific for this time
5′/0′	359	1,029	472	34.0	259	18.6
15′/0′	698	690	226	16.3	68	4.9
15′/15′	812	576	204	14.7	30	2.2
15′/45′	877	511	178	12.8	54	3.9
15′/105′	937	451	159	11.5	38	2.7
15′/165′	897	491	149	10.7	41	3.0
Sum			1,388	100.0	490	35.3
Average	763	625	231	16.7		

titate the number of purified phagosomes by measuring light scattering in the fraction collected from the sucrose gradient. This measure is exquisitely precise and allows us to adjust the phagosome fractions for identical concentration of phagosomes. This is further demonstrated both by the almost identical protein concentration measured in each normalized fraction (data not shown) and the equal loading of total proteins on one-dimensional gels (16, 35). We concluded that the total amount of protein per phagosome does not vary significantly throughout maturation (less than 15%) and is ~12 $\mu g/10^9$ phagosomes. Therefore, each 2D gel of the series was loaded with an equal amount of phagosomes and of total protein and stained to a similar extent. Fig. 2 presents a gallery of 2D gels of phagosome extracts obtained at six time points including a 5-min pulse (5′/0′), a 15-min pulse (15′/0′), and 15-min (15′/15′), 45-min (15′/45′), 105-min (15′/105′), and 165-min (15′/165′) chases after a 15-min pulse. The *colored circles* around the spots indicate a difference compared with the preceding time point: *red circles* indicate spots that increased more than 2-fold in intensity, whereas *green circles* indicate spots that decreased more than 2-fold in intensity. (The spots that were detected at all time points (in varying amounts) are circled in blue in Supplemental Fig. S1.)

This simple analysis revealed substantial remodeling during the different phases. For example, the 5-min pulse (Fig. 2*A*) had the greatest number of different spots (1,029); of these, 259 were specific for this time point (more than at any other time point) (Table II). This complexity at early times likely reflects the fact that early phagosomes contain both proteins derived from the plasma membrane and newly recruited phagosome-specific proteins (16). Not surprisingly, comparison of the second time point with the first revealed the disappearance of 469 spots and appearance of 130 others (Table III). This substantial remodeling likely includes sorting to recycle plasma membrane proteins back to the surface (55, 56). Overall the total number of spots detected decreased over time except at the last time point (Table II). Vast remodeling of the phagosomes during maturation was indicated by the fact that, on average, 184 spots appeared and 291 spots disappeared between any two consecutive time points (Table III). Again on average, 35% of the spots detected were present only at one time point, 20% were detected at only two time points, and 7% were detected at five time points. Nevertheless 12% of all spots were present at all six time points (Supplemental Fig. S1 and Table IV).

TABLE III
Changes between time points

Time points	Appearing	Disappearing	Staying	Percentage staying
5′/0′ *vs.* 15′/0′	130	469	560	54.4
15′/0′ *vs.* 15′/15′	178	292	398	57.7
15′/15′ *vs.* 15′/45′	194	259	317	55.0
15′/45′ *vs.* 15′/105′	198	258	253	49.5
15′/105′ *vs.* 15′/165′	219	179	272	60.3
Average	184	291	360	55.4

TABLE IV
Detection statistics

Number of detections	Number of spots	Percentage
1	490	35.3
2	280	20.2
3	195	14.0
4	164	11.8
5	97	7.0
6	162	11.7
Sum	1,388	100.0

In summary, this analysis clearly indicates distinct phases in the maturation program. We detected the most remodeling at the beginning and end of the pathway and thus propose that uptake and exocytosis are the most complex "multidisciplinary" stages, requiring integration of signaling, membrane trafficking, and cytoskeleton reorganization. The more "specialized" intermediate stages, we suggest, are more uniquely devoted to successive membrane trafficking steps necessary for efficient accumulation of digestive enzymes and extraction and transport of nutrients and may thus require a simpler repertoire of proteins.

Temporal Changes in Phagosome Components—The complexity of the maturation process can be seen from Fig. 3. The reference gel (Fig. 3*A*) shows an overlay of the 1,388 spots detected in the whole time series superimposed on the gel of time point 5′/0′. Spots that were present at two or more time

points are *circled* in *blue* or *red*; the 125 spots *circled* in *red* correspond to proteins identified from the preparative gels (see Table I, column "Group"). The 490 spots present at only one time point are circled in *green*. Although these spots include proteins that potentially are the most stage-specific, they are also most prone to artifact (degradation and spots that could not be matched to other gels), therefore they were not all included in the cluster analysis; instead six spots representative of the proteins that appear only at one of each of the six time points were included. The spots *circled* in *blue* or *red* were analyzed further to monitor how their intensity changed over time. Spot intensities were quantified by densitometry, normalized for the complete temporal profile, and depicted as heat maps in which *red* corresponds to high intensity and *green* corresponds to low intensity (see "Experimental Procedures"). To extend the 2D gel data, we also analyzed the pulse-chased phagosome preparations for the presence of known endosomal and phagosomal proteins by using quantitative Western blotting (Fig. 3*C*). This approach also allowed us to compare the data obtained for a selection of seven proteins by both Western blotting and 2D gels (see below). Again signal intensities were quantified by densitometry, normalized for the temporal profile, and depicted as heat maps (Fig. 3*D*).

Altogether we obtained 925 profiles (for 898 spots present at more than one time point, plus the profiles of the six spots representative of the 490 stage-specific spots, plus the 21 profiles obtained by Western blotting) representing 5,550 individual intensity measurements that are presented in the heat map in Fig. 3*B*. These "temporal profiles" were submitted to cluster analysis, a method also used to group microarray "expression profiles" according to their degree of similarity. Exploratory analysis using a variety of clustering methods and distance metrics gave fairly robust results and similar clusters and revealed that the profiles do not fall into a well defined number of well separated groups. Therefore, the optimal number of clusters was determined so that it would result in (*a*) a relatively homogeneous number of profiles per group (Fig. 4*A*), (*b*) fairly distinct average group profiles (as judged by inspection and by cross-correlation (Fig. 4*B*), see below), and (*c*) rather homogeneous groups (as judged by the standard deviation from the average group profile, Fig. 5 and Supplemental Fig. S3). Finally we used the partition around medoids (PAM) algorithm (46) to classify the 925 profiles into 24 groups (a detailed argument is presented in the supplemental information and Supplemental Fig. S2). At a higher level in the dendrogram there are five major clusters (Fig. 4, *I–V*) that correspond roughly to different times of maximal abundance of each protein during the maturation program.

Many of the 24 groups had simple average profiles, consistent with the proteins they represent having a major function at one stage of phagocytosis and with a relatively simple, linear model of phagosome maturation (Fig. 4*C*). For example, groups 1–6 had a major sharp peak of *red* (high spot intensity) and could easily be aligned in such a sequence in association with groups that have a slightly broader peaks (groups 8, 10, 19, and 22). About a fifth of the groups (groups 7, 9, 12, 13, and 17) comprise proteins that appeared at two stages of maturation, including the first time point for four of them. At the other extreme, some groups (groups 11, 16, 18, 20, and 21) comprise proteins present at most time points, perhaps reflecting an unchanging feature of phagosomes identity or a recurrent function. Finally some groups (groups 14, 15, 23, and 24) comprise proteins that appeared and disappeared from the maturing phagosomes in more complex ways, reflecting either a periodic need for a specific function or the existence of parallel maturation pathways in which they act at different times.

From Temporal Profiling to Functional Grouping—Cluster analysis revealed that the 24 groups are organized into five major clusters that are apparent on the tree structure (Fig. 4*A*, *clusters I–V*) and are also visible on the cross-correlation map as *square regions* of "hot" colors aligned along the *diagonal* (Fig. 4*B*, *boxes*). The groups inside each cluster share a major peak at a common time point, and this reflects the fact that the clusters (from I to V) can be roughly aligned along an axis of maturation in order of appearance of that major peak. This finding is also consistent with a simple, linear model of phagosome maturation as illustrated in Fig. 4*C*, but more complex alternative pathways of maturation are discussed below.

A detailed description of clusters, groups, and proposed associated functions in maturation is presented in the supplemental information, and the composition of each group is presented in Supplemental Figs. S2-1 to S2-6. Briefly looking at cluster I (groups 1, 2, 8, and 11) and the earliest time point, the presence of group 1 proteins reflects the involvement of the actin cytoskeleton, membrane trafficking, and molecules that bridge the two functions to trigger and carry out uptake; group 11 includes many enzymes, probably reflecting the early establishment of the degradative phases of phagocytosis, and group 8 includes $G\alpha_4$, suggesting a signaling function during uptake (see below). Cluster II (groups 3, 9, 14, and 18) comprises a diverse collection of proteins likely reflecting the metabolic role of the phagosome as well as other functions that were proposed recently (see below). Cluster III (groups 4, 7, 12, 16, and 20) reflects functions related to late endosomes and multivesicular body formation, including the necessary signaling, cytoskeleton, and membrane trafficking machinery. The proteins representative of cluster IV (from groups 5, 13, 15, 21, and 22) also reflect late endosomal/lysosomal characteristics featuring digestive components as well as the components of trafficking associated with recycling/exocytosis. Cluster V (groups 6, 17, 19, 23, and 24) completes this series, finishing the evolution started in cluster IV, with the presence of factors typical of late endosomes and recycling/exocytosis, but the prominent digestive character of cluster IV is missing.

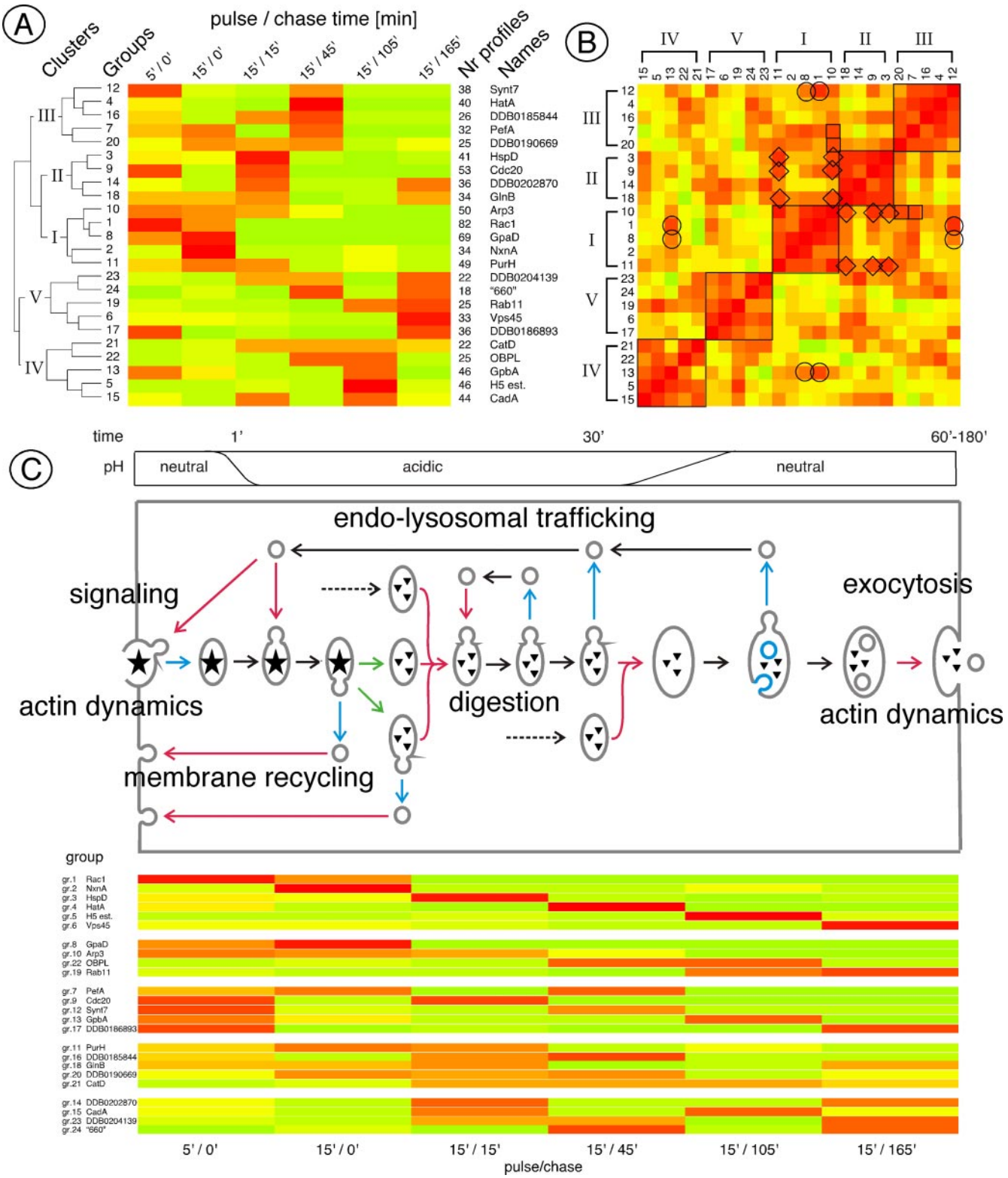

FIG. 4. **Clustering and cross-correlation analyses of temporal profiles and flow chart of phagosome maturation.** *A*, heat map resulting from cluster analysis of 925 temporal profiles and showing the average intensities over the six time points of the 24 groups of proteins indicated on the *left* by a *Roman numeral* (*Groups*). The number of profiles in each group (*Nr profiles*) and their attributed name (*Names*) are indicated on the *right*. The tree on the *left* also illustrates the computed relatedness of the groups and their organization into five clusters (clusters I–V). We named each group according to one representative known protein. When no known and studied protein was present in the group, we

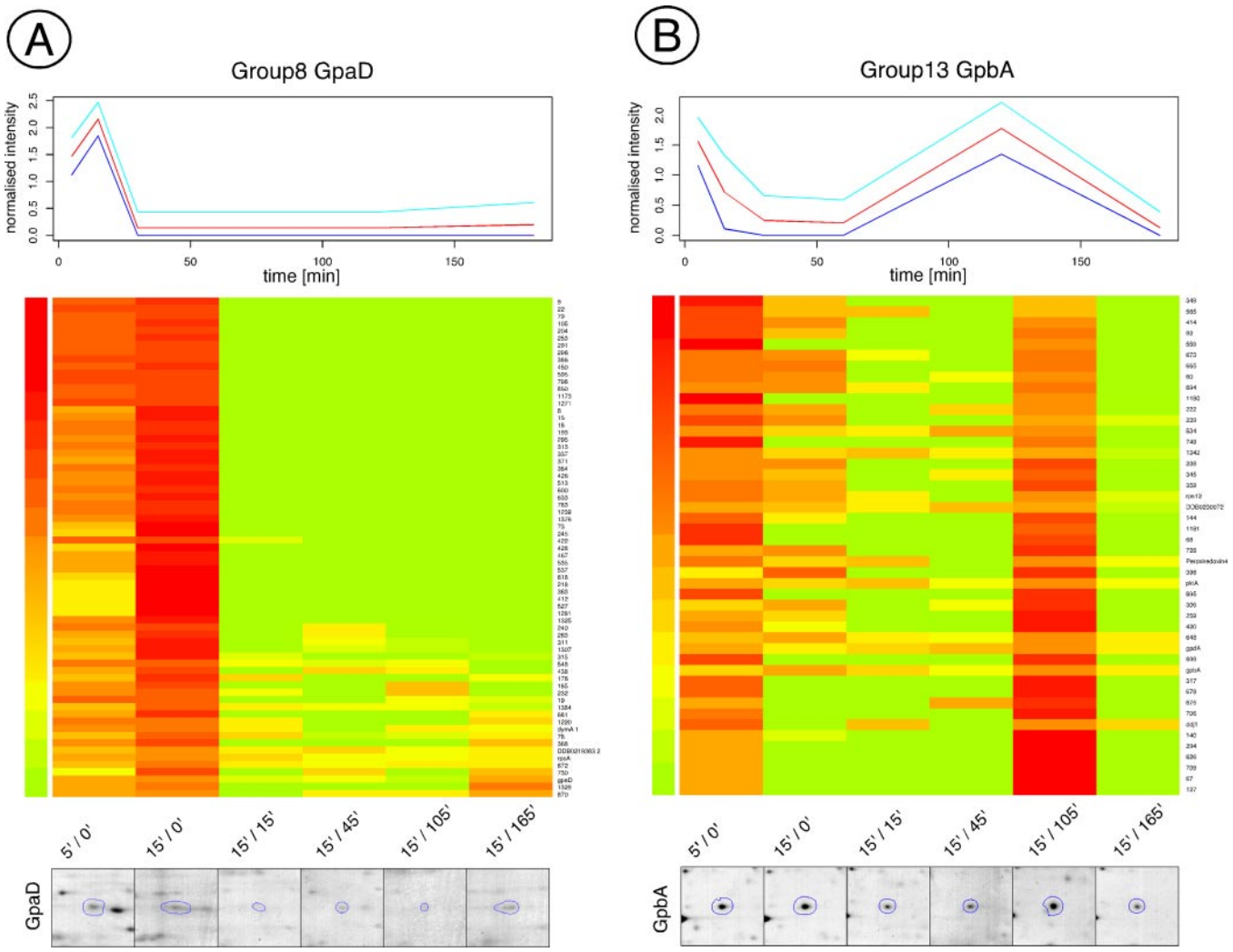

FIG. 5. **Two examples of groups.** Two of the 24 groups (see complete Supplemental Fig. S3) are illustrated here. Group 8 GpaD (*A*) includes Gα_4, three other identified proteins, and 65 unidentified spots, whereas group 13 GpbA (*B*) includes Gβ, six other identified proteins, and 40 unidentified spots. The *top panel* shows the average temporal profile of the group (*red line*) plus or minus one standard deviation (*light* and *dark blue*, respectively), the *middle panel* shows the heat map of the profiles of all group members, and the *bottom panel* shows a portion of each gel of the time series (see Fig. 2) containing one representative spot from the group. Data for the other 22 groups are given in Supplemental Figs. S3-1 to S3-6. (Note that the timescale in the diagram on *top* is linear, whereas the spots and clusters are discrete time points, resulting in a slight shift of alignment.)

Cross-correlation Analysis Reveals Further Relatedness between Functional Groups—Although clustering is important to integrate the information and reveal order in large datasets, a well known and inherent feature of most clustering methods is that sometimes related profiles end up in relatively distant clusters/groups. Therefore, to extend and strengthen the clustering data, we calculated what we call cross-correlation, that is all the pairwise correlation coefficients between the average profiles across all 24 groups. This analysis quantitates and highlights the strength of the relationship between

attributed a name based on the dictyBase identification number. Group 24 contained no identified protein and was thus named after spot 660, which has a representative profile. *B*, heat map matrix of pairwise cross-correlation between the groups indicated by the *Arabic numerals* along the *top* and *left sides*. *Red* indicates identity, and the "*cooler colors*" indicate less relatedness. Clusters are indicated by *Roman numerals* on the *left* and by *boxes* along the *diagonal*. Additional strong correlations are emphasized by *circles*, *squares*, and *diamonds* (see main text). *C*, the scheme in the *central panel* illustrates the various phases of phagosome maturation from uptake of particles (*stars* on the *left*) to the final egestion of undigested remnants (*small triangles* on the *right*). *Arrows* indicate pathways of membrane traffic and crucial processes accompanying the various phases of maturation. The *upper panel* indicates the timing of acidification and neutralization. This scheme is based on one published previously for macropinocytosis (69). The *lower panel* shows the heat maps of the average temporal profiles of the 24 groups indicated at the *left*, illustrating the stages of the maturation program at which these groups of proteins are present.

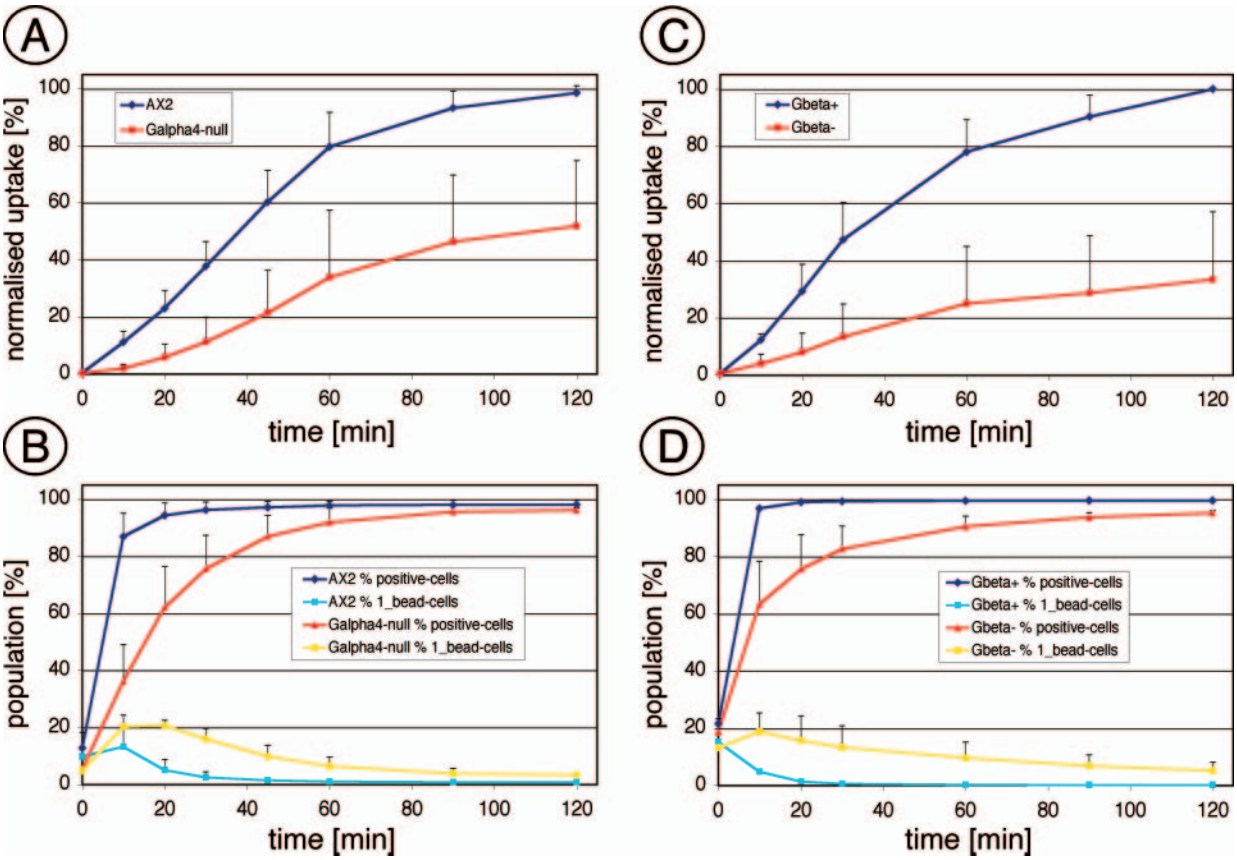

FIG. 6. **Quantification of phagocytosis in two *Dictyostelium* G protein mutants.** Time courses of the phagocytic uptake of 1-μm fluorescent microspheres by various strains of *Dictyostelium* are shown. *A*, fluorescence uptake by Gα_4-null cells (*red curve*) and wild-type cells (*blue curve*) measured by flow cytometry. *C*, fluorescence uptake by Gβ-null cells (*red curve*) and Gβ+ cells (*blue curve*) (see main text for details). Uptake was normalized to wild-type cells or Gβ+ cells, respectively. *B* and *D* show the proportion of cells that acquired one or more beads (*red* and *dark blue curves*) and the proportion of cells that contained one bead only (*yellow* and *light blue curves*). The *red* and *yellow curves* indicate data for the mutant cell lines, and the *dark* and *light blue curves* indicate data for the wild-type and Gβ+ cells. Uptake was assayed in triplicate, and *error bars* represent standard deviations.

any two average temporal profiles of contiguous or non-contiguous groups of the hierarchical clustering tree. On the resulting heat map matrix (Fig. 4*B*), the index of correlation between the average temporal profiles of two groups is indicated at the intersection by a color-coded square. *Red* (on the *diagonal*) indicates identity, and decreasing similarity is indicated by colors that become closer to *green*.

The cross-correlation map reveals additional relatedness between groups outside the major five clusters, visible as isolated or small groups of hot *squares* off the *diagonal* (Fig. 4*B*, emphasized by *circles*, *squares*, and *diamonds*). For example, groups 1, 8, 12, and 13 are highly related (Fig. 4*B*, *circles*). In addition to the proteins already mentioned above, group 12 also contains signaling and membrane trafficking proteins, and group 13 also contains some enzymes. Similarly groups 10 and 11 from cluster I are closely related to groups 3, 9, and 18 from cluster II, and finally group 10 from cluster I is related to groups 7 and 20 from cluster III. Overall it appears that group 10 has a remarkable position, being a close relative of many groups, both inside and outside its cluster. Altogether these complex patterns of appearance and disappearance of some protein groups during maturation emphasize that the linear maturation program depicted in Fig. 4*C* is an oversimplification and should be completed by complex cross-talk between endocytic and phagocytic organelles and/or the existence of alternative parallel maturation pathways (57).

We also focused on proteins for which we had both Western blotting and spot quantification data. For example, the profiles obtained for vacuolin by Western blotting (with an antibody that recognizes both vacA and vacB (58)) and for the vacA spot both fall into group 19, but the profile for vacB is in group 15. These groups are in two different but related clusters (IV and V) and also show a relatively strong cross-correlation (Fig. 4*B*, see the intersection of groups 19 and 15). The profiles obtained for coronin by Western blotting (group 1) and for the CorA spot (group 11) fall into different groups of the same cluster (cluster I), but these groups are among those with highly cross-correlated average profiles. Similarly the profile obtained for Gβ by Western blotting (group 1) and the

corresponding GpbA spot (group 13) are neither in the same group nor the same cluster (clusters I and IV, respectively) but show highest pairwise cross-correlation. These data demonstrate that the use of different methods to obtain the temporal profiles can result in some degree of discrepancy and thus show some of the limitations of our approach. Nevertheless the discrepancies are small and do not really affect our overall conclusions and the concept presented here.

Our analysis of time-dependent proteomics data has allowed us to establish a model of phagocytic mechanisms that will be useful for further functional analysis in *Dictyostelium* and other organisms. We next aimed to test a prediction of this model as a proof of principle for future investigations.

Heterotrimeric G Protein Function in Early Phagocytosis—Many signaling pathways are activated when a ligand binds to its G protein-coupled receptor; this receptor-ligand binding activates the downstream heterotrimeric G protein (consisting of one α, one β, and one γ subunit) thus converting the extracellular signal into an intracellular response. Subunits of trimeric G proteins have been reported in phagosomes from mouse (11) and *E. histolytica* (31), and a study based on use of inhibitors and toxins has found evidence for a role during phagocytosis (59). The latter data are contradicted by a recent report that knock-down of multiple Gβ and Gγ in a macrophage line abolished G protein-coupled signaling without affecting phagocytosis (60). In *Dictyostelium*, there are 14 different Gα subunits, one Gβ and one Gβ-like subunit (12), and one Gγ subunit. G proteins are essential in this organism for chemotaxis, cell aggregation, and differentiation. In particular, Gα_2 (61) and Gα_4 (62, 63) are important for chemotaxis and differentiation, but no Gα has been shown to play a role in phagocytosis. Gβ, on the other hand, is required for chemotactic responses and multicellular development as well as phagocytosis (64–66).

On our 2D gels, there was a strong signal from Gα_4 at the two earliest time points (Fig. 5*A*, *lower panel*) suggesting that it may be involved in phagocytic uptake. Likewise group 13 proteins, including Gβ (GpbA), were also present around the beginning of phagocytosis (Fig. 5*B*). Interestingly both Gα_4 and Gβ also peaked at a later time point, perhaps indicating a dual role both during the early uptake phase and in a late maturation phase that might reflect the documented role of Gβ in actin reorganization (66) and the function of the actin cytoskeleton in both uptake and exocytosis (67). Because of its presence on early phagosomes, we wondered whether Gα_4 might also play a role in uptake similar to the function reported for Gβ in phagocytosis (66) and thus might be one missing link upstream of Gβ linking the G$\alpha\beta\gamma$ complex to an unknown receptor. We therefore compared phagocytosis in cells deficient in Gα_4 subunit (Gα_4-null cells) with wild-type cells (Ax2 cells) and, as a positive control, cells deficient in Gβ subunit (Gβ-null cells) with cells expressing a fully functional His-tagged form of the Gβ (Gβ+). To do so, we used a flow cytometry-based particle uptake assay to monitor the uptake kinetics of brightly fluorescent beads (see "Experimental Procedures"). The knock-out strains grew at rates indistinguishable from their respective controls, demonstrating their relative fitness. Both mutant cell lines had a pronounced defect in bead uptake (Fig. 6). During the 120-min course of the assay, the Gα_4-null cell population showed an uptake rate of fluorescent beads 50% lower than that of the wild-type cells (Fig. 6*A*), and the rate of uptake in the Gβ-null cell population was reduced to 40% of that of the Gβ+ cells (Fig. 6*C*). All the cells in both mutant strains possessed some phagocytic activity and were able to ingest at least one particle at a rate only slightly slower than their respective controls (Fig. 6, *B* and *D*, *red curves* compared with *dark blue curves*). By contrast, the phagocytic rate in both mutant strains was markedly slower than in the controls when the proportion of cells containing only one bead was plotted against time. In the wild-type and Gβ+ strains, this population appeared and disappeared rapidly (Fig. 6, *B* and *D*, *light blue curves*), whereas in both mutant strains (*yellow curves*), the peak of cells with only one bead appeared later and disappeared only slowly, illustrating the lower initial rate of uptake of both the first and second bead. We therefore conclude that both Gα_4-null and Gβ-null strains are inefficient in an early step of phagocytosis, unambiguously implicating a Gα in this mechanism. A similar functional analysis can now be performed for the proteins of unknown function in these groups with the aim of both validating our approach and strengthening the understanding of the role of heterotrimeric G proteins in phagocytic uptake. The strategy can equally be expanded to any other group of phagosome proteins.

Acknowledgments—We thank all the laboratory members who contributed thoughts and comments to this investigation as well as help with phagosome purification, in particular Hans-Jörg Warnatz, Eva Neuhaus, and Régis Dieckmann.

* This work was supported in part by the Max Planck Society, The Wellcome Trust, and the Swiss National Science Foundation (to T. S.). The costs of publication of this article were defrayed in part by the payment of page charges. This article must therefore be hereby marked "*advertisement*" in accordance with 18 U.S.C. Section 1734 solely to indicate this fact.

S The on-line version of this article (available at http://www.mcponline.org) contains supplemental material.

[c] Both authors contributed equally to this work.

[h] Supported by the National Centre of Competence in Research (NCCR) Molecular Oncology, a research program of the Swiss National Science Foundation.

[j] To whom correspondence should be addressed. Tel.: 41-22-379-6496; Fax: 41-22-379-6470; E-mail: thierry.soldati@biochem.unige.ch.

REFERENCES

1. Desjardins, M., Huber, L. A., Parton, R. G., and Griffiths, G. (1994) Biogenesis of phagolysosomes proceeds through a sequential series of interactions with the endocytic apparatus. *J. Cell Biol.* **124,** 677–688
2. Jutras, I., and Desjardins, M. (2005) Phagocytosis: at the crossroads of innate and adaptive immunity. *Annu. Rev. Cell Dev. Biol.* **21,** 511–527
3. Botelho, R. J., Scott, C. C., and Grinstein, S. (2004) Phosphoinositide involvement in phagocytosis and phagosome maturation. *Curr. Top.*

Microbiol. Immunol. **282,** 1–30
4. Anes, E., Kuhnel, M. P., Bos, E., Moniz-Pereira, J., Habermann, A., and Griffiths, G. (2003) Selected lipids activate phagosome actin assembly and maturation resulting in killing of pathogenic mycobacteria. *Nat. Cell Biol.* **5,** 793–802
5. Niedergang, F., and Chavrier, P. (2005) Regulation of phagocytosis by Rho GTPases. *Curr. Top. Microbiol. Immunol*. **291,** 43–60
6. Niedergang, F., and Chavrier, P. (2004) Signaling and membrane dynamics during phagocytosis: many roads lead to the phagos(R)ome. *Curr. Opin. Cell Biol.* **16,** 422–428
7. Castellano, F., Chavrier, P., and Caron, E. (2001) Actin dynamics during phagocytosis. *Semin. Immunol*. **13,** 347–355
8. Bajno, L., Peng, X. R., Schreiber, A. D., Moore, H. P., Trimble, W. S., and Grinstein, S. (2000) Focal exocytosis of VAMP3-containing vesicles at sites of phagosome formation. *J. Cell Biol.* **149,** 697–706
9. Braun, V., Fraisier, V., Raposo, G., Hurbain, I., Sibarita, J. B., Chavrier, P., Galli, T., and Niedergang, F. (2004) TI-VAMP/VAMP7 is required for optimal phagocytosis of opsonised particles in macrophages. *EMBO J.* **23,** 4166–4176
10. Desjardins, M., Houde, M., and Gagnon, E. (2005) Phagocytosis: the convoluted way from nutrition to adaptive immunity. *Immunol. Rev.* **207,** 158–165
11. Garin, J., Diez, R., Kieffer, S., Dermine, J.F., Duclos, S., Gagnon, E., Sadoul, R., Rondeau, C., and Desjardins, M. (2001) The phagosome proteome: insight into phagosome functions. *J. Cell Biol.* **152,** 165–180
12. Eichinger, L., Pachebat, J. A., Glockner, G., Rajandream, M. A., Sucgang, R., Berriman, M., Song, J., Olsen, R., Szafranski, K., Xu, Q., Tunggal, B., Kummerfeld, S., Madera, M., Konfortov, B. A., Rivero, F., Bankier, A. T., Lehmann, R., Hamlin, N., Davies, R., Gaudet, P., Fey, P., Pilcher, K., Chen, G., Saunders, D., Sodergren, E., Davis, P., Kerhornou, A., Nie, X., Hall, N., Anjard, C., Hemphill, L., Bason, N., Farbrother, P., Desany, B., Just, E., Morio, T., Rost, R., Churcher, C., Cooper, J., Haydock, S., van Driessche, N., Cronin, A., Goodhead, I., Muzny, D., Mourier, T., Pain, A., Lu, M., Harper, D., Lindsay, R., Hauser, H., James, K., Quiles, M., Madan Babu, M., Saito, T., Buchrieser, C., Wardroper, A., Felder, M., Thangavelu, M., Johnson, D., Knights, A., Loulseged, H., Mungall, K., Oliver, K., Price, C., Quail, M. A., Urushihara, H., Hernandez, J., Rabbinowitsch, E., Steffen, D., Sanders, M., Ma, J., Kohara, Y., Sharp, S., Simmonds, M., Spiegler, S., Tivey, A., Sugano, S., White, B., Walker, D., Woodward, J., Winckler, T., Tanaka, Y., Shaulsky, G., Schleicher, M., Weinstock, G., Rosenthal, A., Cox, E. C., Chisholm, R. L., Gibbs, R., Loomis, W. F., Platzer, M., Kay, R. R., Williams, J., Dear, P. H., Noegel, A. A., Barrell, B., and Kuspa, A. (2005) The genome of the social amoeba Dictyostelium discoideum. *Nature* **435,** 43–57
13. Takeda, K., Saito, T., Tanaka, T., Morio, T., Maeda, M., Tanaka, Y., and Ochiai, H. (2003) A novel gene trap method using terminator-REMI and 3′ rapid amplification of cDNA ends (RACE) in Dictyostelium. *Gene* (*Amst.*) **312,** 321–333
14. Van Driessche, N., Demsar, J., Booth, E. O., Hill, P., Juvan, P., Zupan, B., Kuspa, A., and Shaulsky, G. (2005) Epistasis analysis with global transcriptional phenotypes. *Nat. Genet.* **37,** 471–477
15. Alexander, S., Srinivasan, S., and Alexander, H. (2003) Proteomics opens doors to the mechanisms of developmentally regulated secretion. *Mol. Cell. Proteomics* **2,** 1156–1163
16. Gotthardt, D., Warnatz, H. J., Henschel, O., Bruckert, F., Schleicher, M., and Soldati, T. (2002) High-resolution dissection of phagosome maturation reveals distinct membrane trafficking phases. *Mol. Biol. Cell* **13,** 3508–3520
17. Steinert, M., and Heuner, K. (2005) Dictyostelium as host model for pathogenesis. *Cell. Microbiol*. **7,** 307–314
18. Chen, J., de Felipe, K. S., Clarke, M., Lu, H., Anderson, O. R., Segal, G., and Shuman, H. A. (2004) Legionella effectors that promote nonlytic release from protozoa. *Science* **303,** 1358–1361
19. Solomon, J. M., Rupper, A., Cardelli, J. A., and Isberg, R. R. (2000) Intracellular growth of Legionella pneumophila in Dictyostelium discoideum, a system for genetic analysis of host-pathogen interactions. *Infect. Immun*. **68,** 2939–2947
20. Solomon, J. M., Leung, G. S., and Isberg, R. R. (2003) Intracellular replication of Mycobacterium marinum within Dictyostelium discoideum: efficient replication in the absence of host coronin. *Infect. Immun*. **71,** 3578–3586
21. Cosson, P., Zulianello, L., Join-Lambert, O., Faurisson, F., Gebbie, L., Benghezal, M., Van Delden, C., Curty, L. K., and Kohler, T. (2002) Pseudomonas aeruginosa virulence analyzed in a Dictyostelium discoideum host system. *J. Bacteriol*. **184,** 3027–3033
22. Pukatzki, S., Kessin, R. H., and Mekalanos, J. J. (2002) The human pathogen Pseudomonas aeruginosa utilizes conserved virulence pathways to infect the social amoeba Dictyostelium discoideum. *Proc. Natl. Acad. Sci. U. S. A.* **99,** 3159–3164
23. Cardelli, J. (2001) Phagocytosis and macropinocytosis in Dictyostelium: phosphoinositide-based processes, biochemically distinct. *Traffic* **2,** 311–320
24. Duhon, D., and Cardelli, J. (2002) The regulation of phagosome maturation in Dictyostelium. *J. Muscle Res. Cell Motil*. **23,** 803–808
25. Maniak, M. (2002) Conserved features of endocytosis in Dictyostelium. *Int. Rev. Cytol*. **221,** 257–287
26. Neuhaus, E. M., Almers, W., and Soldati, T. (2002) Morphology and dynamics of the endocytic pathway in Dictyostelium discoideum. *Mol. Biol. Cell* **13,** 1390–1407
27. Steinert, M., Leippe, M., and Roeder, T. (2003) Surrogate hosts: protozoa and invertebrates as models for studying pathogen-host interactions. *Int. J. Med. Microbiol*. **293,** 321–332
28. Marion, S., Voigt, H., and Guillen, N. (2000) Cellular and biochemical analysis of phagocytosis in Entamoeba histolytica. *Arch. Med. Res*. **31,** S178–S180
29. Mitra, B. N., Yasuda, T., Kobayashi, S., Saito-Nakano, Y., and Nozaki, T. (2005) Differences in morphology of phagosomes and kinetics of acidification and degradation in phagosomes between the pathogenic Entamoeba histolytica and the non-pathogenic Entamoeba dispar. *Cell. Motil. Cytoskelet.* **62,** 84–99
30. Okada, M., Huston, C. D., Mann, B. J., Petri, W. A., Jr., Kita, K., and Nozaki, T. (2005) Proteomic analysis of phagocytosis in the enteric protozoan parasite Entamoeba histolytica. *Eukaryot. Cell* **4,** 827–831
31. Marion, S., Laurent, C., and Guillen, N. (2005) Signalization and cytoskeleton activity through myosin IB during the early steps of phagocytosis in Entamoeba histolytica: a proteomic approach. *Cell. Microbiol*. **7,** 1504–1518
32. Sussman, M. (1987) Cultivation and synchronous morphogenesis of Dictyostelium under controlled experimental conditions. *Methods Cell Biol.* **28,** 9–29
33. Laemmli, U. K. (1970) Cleavage of structural proteins during the assembly of the head of bacteriophage T4. *Nature* **227,** 680–685
34. Schwarz, E. C., Neuhaus, E. M., Kistler, C., Henkel, A. W., and Soldati, T. (2000) Dictyostelium myosin IK is involved in the maintenance of cortical tension and affects motility and phagocytosis. *J. Cell Sci.* **113,** 621–633
35. Gotthardt, D., Dieckmann, R., Blancheteau, V., Kistler, C., Reichardt, F., and Soldati, T. (2006) Preparation of intact, highly purified phagosomes from Dictyostelium. *Methods Mol. Biol. Dictyostelium discoideum Protocols* edited by Eichinger and Rivero, pp. 439–448, Humana Press, Totowa, NJ
36. Wu, C. C., MacCoss, M. J., Howell, K. E., and Yates, J. R., III (2003) A method for the comprehensive proteomic analysis of membrane proteins. *Nat. Biotechnol*. **21,** 532–538
37. Gorg, A., Postel, W., and Gunther, S. (1988) The current state of two-dimensional electrophoresis with immobilized pH gradients. *Electrophoresis* **9,** 531–546
38. Rabilloud, T., Adessi, C., Giraudel, A., and Lunardi, J. (1997) Improvement of the solubilization of proteins in two-dimensional electrophoresis with immobilized pH gradients. *Electrophoresis* **18,** 307–316
39. Gorg, A., Obermaier, C., Boguth, G., Csordas, A., Diaz, J. J., and Madjar, J. J. (1997) Very alkaline immobilized pH gradients for two-dimensional electrophoresis of ribosomal and nuclear proteins. *Electrophoresis* **18,** 328–337
40. Gorg, A., Obermaier, C., Boguth, G., Harder, A., Scheibe, B., Wildgruber, R., and Weiss, W. (2000) The current state of two-dimensional electrophoresis with immobilized pH gradients. *Electrophoresis* **21,** 1037–1053
41. Gorg, A., and Weiss, W. (1999) Analytical IPG-Dalt. *Methods Mol. Biol*. **112,** 189–195
42. Regula, J. T., Ueberle, B., Boguth, G., Gorg, A., Schnolzer, M., Herrmann, R., and Frank, R. (2000) Towards a two-dimensional proteome map of Mycoplasma pneumoniae. *Electrophoresis* **21,** 3765–3780
43. Blum, H., Beier, H., and Gross, H. J. (1987) Improved silver staining of

plant-proteins, RNA and DNA in polyacrylamide gels. *Electrophoresis* **8,** 93–99
44. Catrein, I., Herrmann, R., Bosserhoff, A., and Ruppert, T. (2005) Experimental proof for a signal peptidase I like activity in Mycoplasma pneumoniae, but absence of a gene encoding a conserved bacterial type I SPase. *FEBS J.* **272,** 2892–2900
45. Opitz, C., Di Cristina, M., Reiss, M., Ruppert, T., Crisanti, A., and Soldati, D. (2002) Intramembrane cleavage of microneme proteins at the surface of the apicomplexan parasite Toxoplasma gondii. *EMBO J.* **21,** 1577–1585
46. Kaufman, L., and Rousseuw, P. J. (1990) *Finding Groups in Data: an Introduction to Cluster Analysis,* Wiley-Interscience, New York
47. Chevallet, M., Santoni, V., Poinas, A., Rouquie, D., Fuchs, A., Kieffer, S., Rossignol, M., Lunardi, J., Garin, J., and Rabilloud, T. (1998) New zwitterionic detergents improve the analysis of membrane proteins by two-dimensional electrophoresis. *Electrophoresis* **19,** 1901–1909
48. Harris, E., Yoshida, K., Cardelli, J., and Bush, J. (2001) Rab11-like GTPase associates with and regulates the structure and function of the contractile vacuole system in Dictyostelium. *J. Cell Sci.* **114,** 3035–3045
49. Harris, E., and Cardelli, J. (2002) RabD, a Dictyostelium Rab14-related GTPase, regulates phagocytosis and homotypic phagosome and lysosome fusion. *J. Cell Sci.* **115,** 3703–3713
50. Seastone, D. J., Zhang, L., Buczynski, G., Rebstein, P., Weeks, G., Spiegelman, G., and Cardelli, J. (1999) The small Mr Ras-like GTPase Rap1 and the phospholipase C pathway act to regulate phagocytosis in Dictyostelium discoideum. *Mol. Biol. Cell* **10,** 393–406
51. Scianimanico, S., Desrosiers, M., Dermine, J. F., Meresse, S., Descoteaux, A., and Desjardins, M. (1999) Impaired recruitment of the small GTPase rab7 correlates with the inhibition of phagosome maturation by Leishmania donovani promastigotes. *Cell Microbiol*. **1,** 19–32
52. Uchida, H., Kondo, A., Yoshimura, Y., Mazaki, Y., and Sabe, H. (2001) PAG3/Papα/KIAA0400, a GTPase-activating protein for ADP-ribosylation factor (ARF), regulates ARF6 in Fcγ receptor-mediated phagocytosis of macrophages. *J. Exp. Med.* **193,** 955–966
53. Vega, V. L., and De Maio, A. (2005) Increase in phagocytosis after geldanamycin treatment or heat shock: role of heat shock proteins. *J. Immunol.* **175,** 5280–5287
54. Gagnon, E., Duclos, S., Rondeau, C., Chevet, E., Cameron, P. H., Steele-Mortimer, O., Paiement, J., Bergeron, J. J., and Desjardins, M. (2002) Endoplasmic reticulum-mediated phagocytosis is a mechanism of entry into macrophages. *Cell* **110,** 119–131
55. Ravanel, K., de Chassey, B., Cornillon, S., Benghezal, M., Zulianello, L., Gebbie, L., Letourneur, F., and Cosson, P. (2001) Membrane sorting in the endocytic and phagocytic pathway of Dictyostelium discoideum. *Eur. J. Cell Biol.* **80,** 754–764
56. Neuhaus, E. M., and Soldati, T. (2000) A myosin I is involved in membrane recycling from early endosomes. *J. Cell Biol.* **150,** 1013–1026
57. Griffiths, G. (2004) On phagosome individuality and membrane signalling networks. *Trends Cell Biol.* **14,** 343–351
58. Jenne, N., Rauchenberger, R., Hacker, U., Kast, T., and Maniak, M. (1998) Targeted gene disruption reveals a role for vacuolin B in the late endocytic pathway and exocytosis. *J. Cell Sci.* **111,** 61–70
59. Damiani, M. T., and Colombo, M. I. (2001) Involvement of heterotrimeric G proteins in phagocytosis and recycling from the phagosomal compartment. *Exp. Cell Res.* **271,** 189–199
60. Hwang, J. I., Choi, S., Fraser, I. D., Chang, M. S., and Simon, M. I. (2005) Silencing the expression of multiple Gβ-subunits eliminates signaling mediated by all four families of G proteins. *Proc. Natl. Acad. Sci. U. S. A.* **102,** 9493–9498
61. Natarajan, K., Ashley, C. A., and Hadwiger, J. A. (2000) Related Gα subunits play opposing roles during Dictyostelium development. *Differentiation* **66,** 136–146
62. Hadwiger, J. A., and Firtel, R. A. (1992) Analysis of Gα4, a G-protein subunit required for multicellular development in Dictyostelium. *Genes Dev.* **6,** 38–49
63. Hadwiger, J. A., and Srinivasan, J. (1999) Folic acid stimulation of the Gα4 G protein-mediated signal transduction pathway inhibits anterior prestalk cell development in Dictyostelium. *Differentiation* **64,** 195–204
64. Wu, L., Valkema, R., Van Haastert, P. J., and Devreotes, P. N. (1995) The G protein β subunit is essential for multiple responses to chemoattractants in Dictyostelium. *J. Cell Biol.* **129,** 1667–1675
65. Lilly, P., Wu, L., Welker, D. L., and Devreotes, P. N. (1993) A G-protein β-subunit is essential for Dictyostelium development. *Genes Dev.* **7,** 986–995
66. Peracino, B., Borleis, J., Jin, T., Westphal, M., Schwartz, J. M., Wu, L., Bracco, E., Gerisch, G., Devreotes, P., and Bozzaro, S. (1998) G protein β subunit-null mutants are impaired in phagocytosis and chemotaxis due to inappropriate regulation of the actin cytoskeleton. *J. Cell Biol.* **141,** 1529–1537
67. Lee, E., and Knecht, D. A. (2002) Visualization of actin dynamics during macropinocytosis and exocytosis. *Traffic* **3,** 186–192
68. Lefkir, Y., Malbouyres, M., Gotthardt, D., Ozinsky, A., Cornillon, S., Bruckert, F., Aderem, A. A., Soldati, T., Cosson, P., and Letourneur, F. (2004) Involvement of the AP-1 adaptor complex in early steps of phagocytosis and macropinocytosis. *Mol. Biol. Cell* **15,** 861–869
69. Maniak, M. (2003) Fusion and fission events in the endocytic pathway of Dictyostelium. *Traffic* **4,** 1–5